Microscopic Calculations of the Giant Pairing Vibration in Light Nuclei

F. Barranco

Sevilla University

R.A. Broglia

The Niels Bohr Institute, Copenhagen

G. Potel

Livermore National Laboratory

E. Vigezzi

INFN Milano

The Giant Pairing Vibration seminal paper

Volume 69B, number 2 PHYSICS LETTERS 1 August 1977

HIGH-LYING PAIRING RESONANCES★

R.A. BROGLIA

The Niels Bohr Institute, University of Copenhagen, DK-2100 Copenhagen Ø, Denmark [1]

State University of New York, Department of Physics, Stony Brook, New York 11794, USA

and

D.R. BES[2]

NORDITA, DK-2100 Copenhagen Ø, Denmark

Received 1 April 1977

Pairing vibrations based on the excitation of pairs of particles and holes across major shells are predicted at an excitation energy of about $70/A^{1/3}$ MeV and carrying a cross section which is 20%–100% the ground state cross section.

The Pairing Vibrations; schematic example

$^{16}O \rightarrow {}^{18}O$

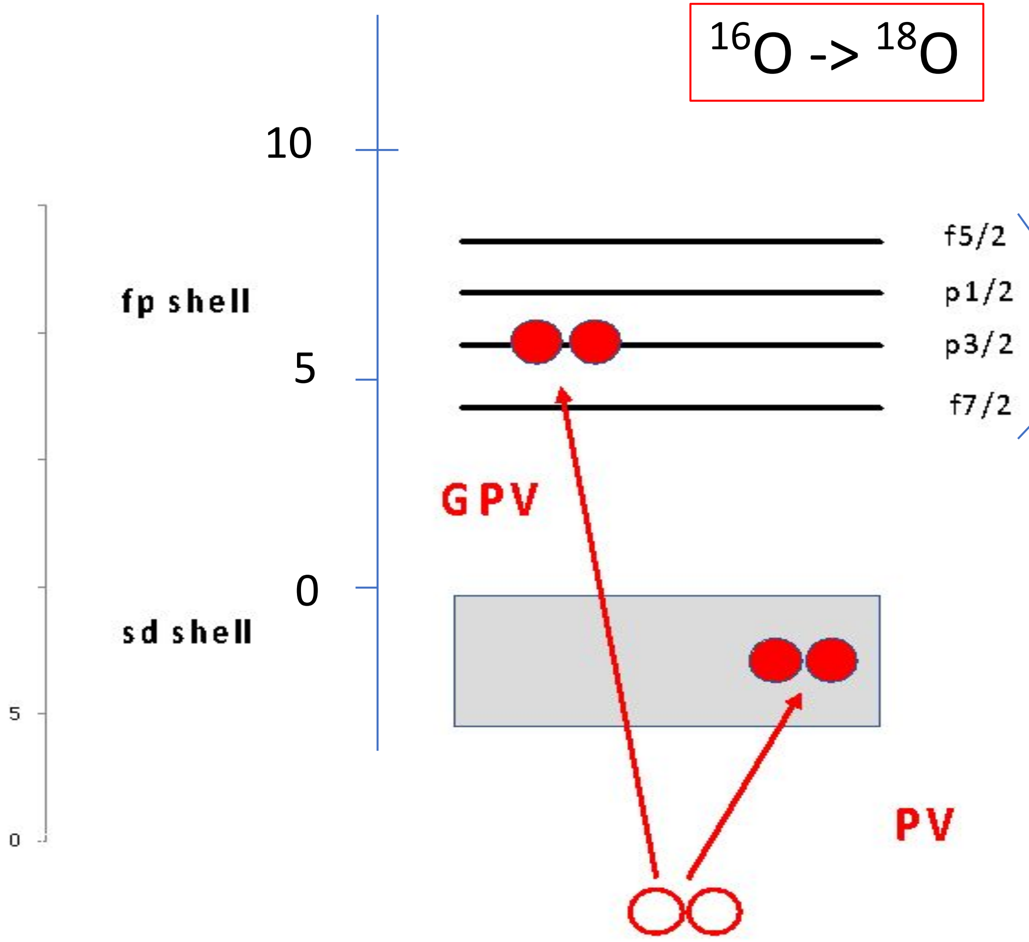

Pairing Interaction □ Coherent mix □ Collectivity

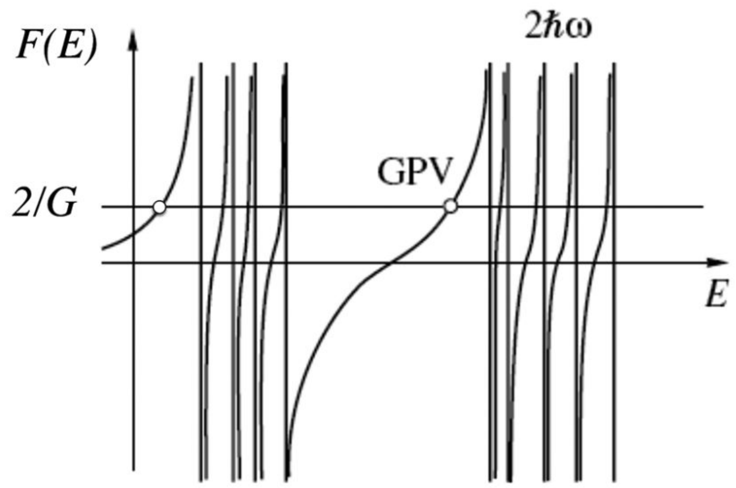

$$\hbar\omega_{GPV} \sim 2\hbar\omega_0 - \Omega G \sim \frac{65MeV}{A^{1/3}}$$

Pair Addition mode

Pair Removal $^{16}O \rightarrow {}^{14}O$ also exist

Low lying PV as a collective mode

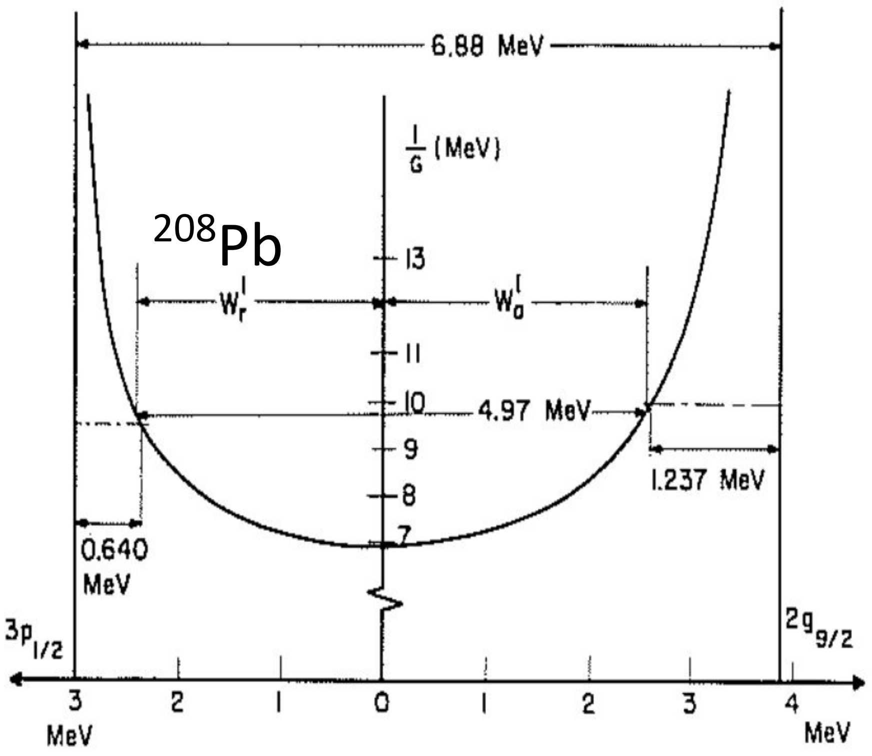

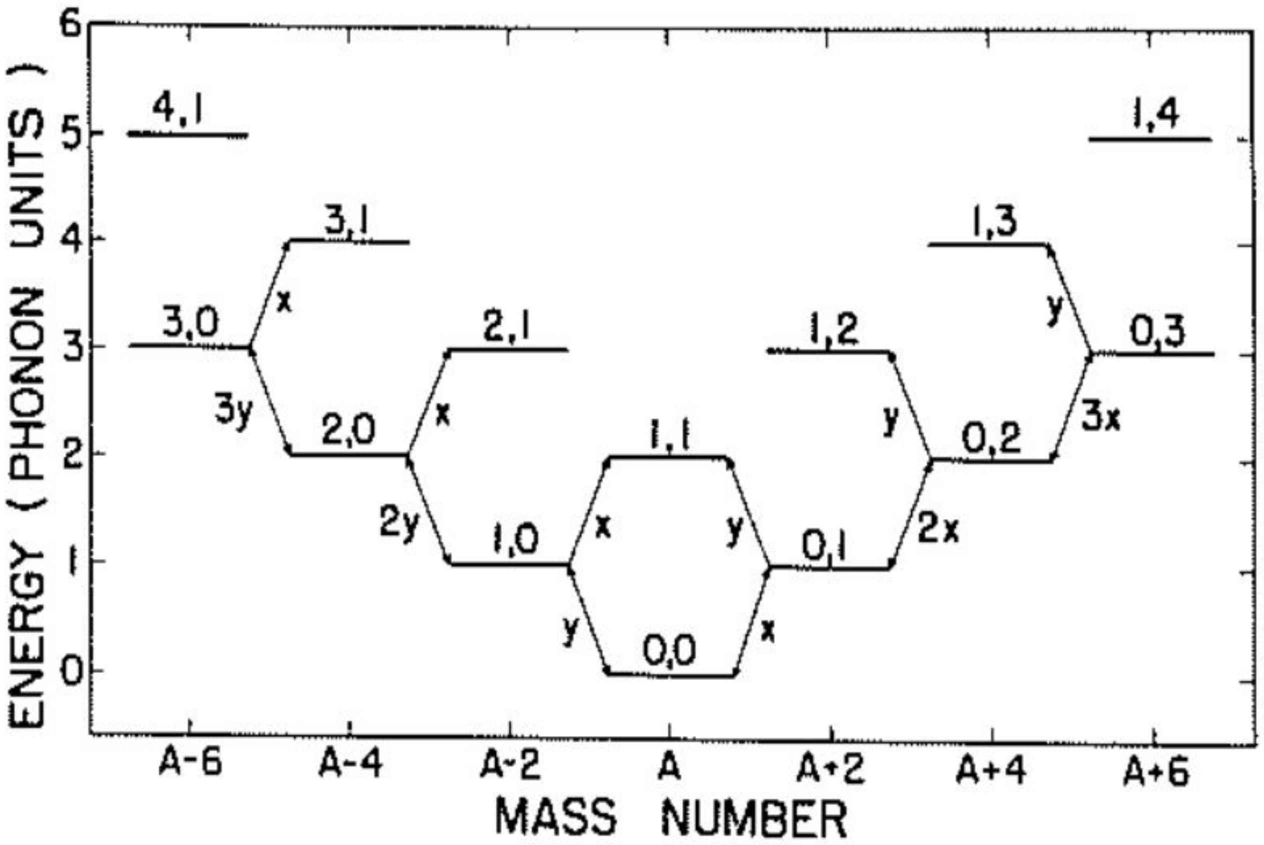

Using the monopole pairing interaction $-GP^+P$
For G large enough ⭢ PHASE TRANSITION (Superfluid)

R.A. Broglia, O. Hansen, C.Riedel, Adv. Nucl. Phys. 6 (1973) 287

Pairing Rotations

The single-particle potential V is not invariant under

rotations in three dimensions	gauge transformations
$R(\mathbf{n},\theta) = \exp\{-i\,\mathbf{I}\cdot\mathbf{n}\theta\}$	$\mathcal{G}(\varphi) = \exp\{-i\,\mathcal{N}\varphi\}$
total angular momentum operator: $\mathbf{I}$	number operator: $\mathcal{N} = \sum_{\nu>0} (c_\nu^+ c_\nu + c_{\bar\nu}^+ c_{\bar\nu})$
$R(\mathbf{n},\theta) Q_\mu R^{-1}(\mathbf{n},\theta) = \sum_{\mu'} D^2_{\mu'\mu}(\omega) Q_{\mu'}$	$\mathcal{G}(\varphi) T(\alpha) \mathcal{G}^{-1}(\varphi) = e^{-i\alpha\varphi} T(\alpha)$
ω = Euler angles	φ = gauge angle
Q = tensor operator of rank two	T = operator with transfer quantum number α

The violation of

spherical symmetry	particle number

defines an intrinsic system of reference in

the physical three-dimensional space	an abstract space

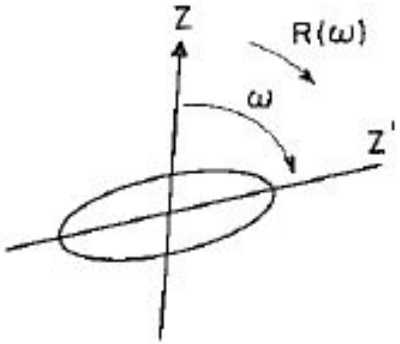

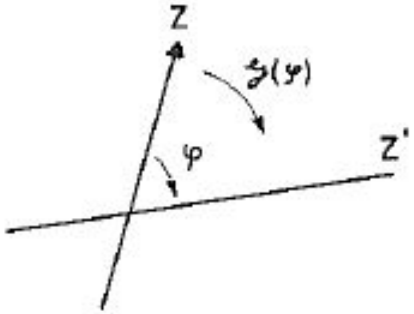

Instead of parametrizing the deformation of the potential by

K_μ	Δ_α

one can use

β and γ and the angle $\boldsymbol{\omega}$	the BCS gap parameter Δ and the angle φ

that defines the orientation of the intrinsic frame of reference.

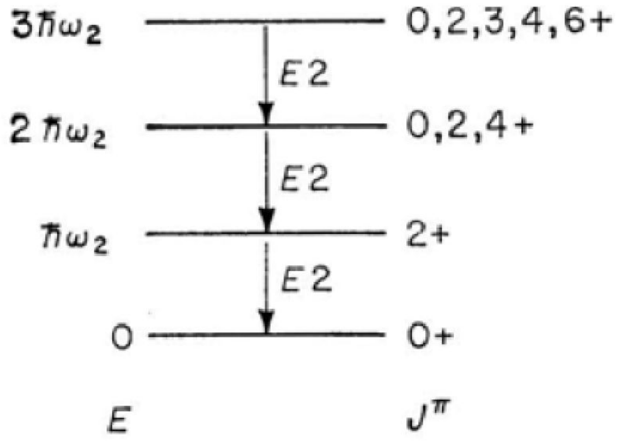

$3\hbar\omega_2$
0,2,3,4,6+
E2
$2\hbar\omega_2$
0,2,4+
E2
$\hbar\omega_2$
2+
E2
0
0+
E
J^π

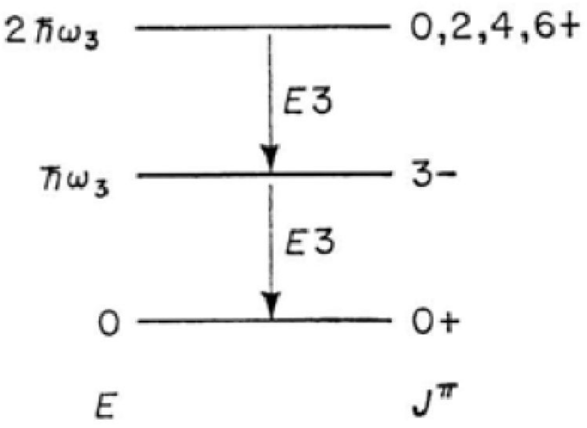

$2\hbar\omega_3$
0,2,4,6+
E3
$\hbar\omega_3$
3−
E3
0
0+
E
J^π

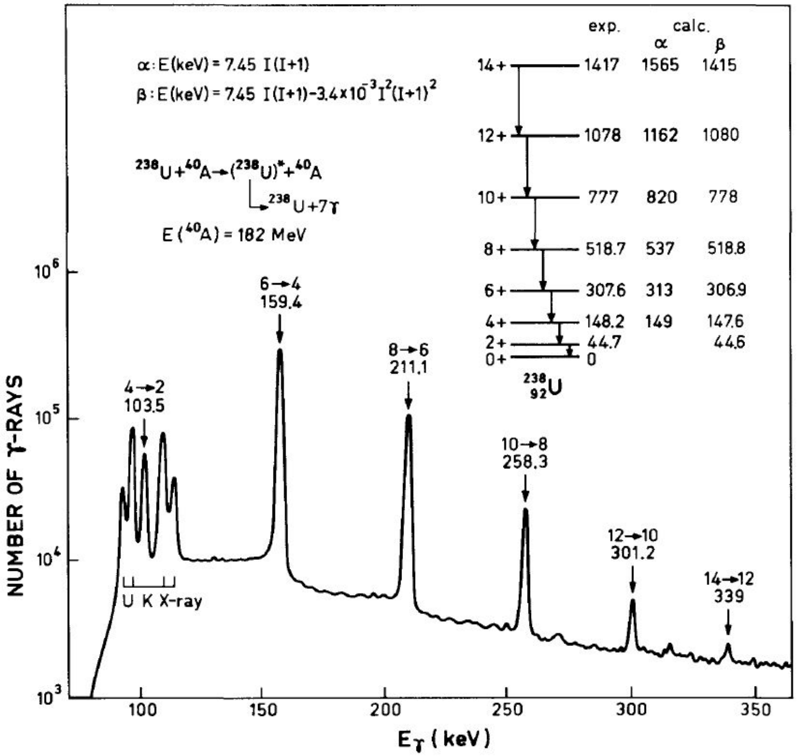

α: E(keV) = 7.45 I(I+1)
β: E(keV) = 7.45 I(I+1)−3.4×10⁻³I²(I+1)²
²³⁸U+⁴⁰A→(²³⁸U)*+⁴⁰A
²³⁸U+7γ
E(⁴⁰A) = 182 MeV
exp.
calc.
α
β
14+ 1417 1565 1415
12+ 1078 1162 1080
10+ 777 820 778
8+ 518.7 537 518.8
6+ 307.6 313 306.9
4+ 148.2 149 147.6
2+ 44.7 44.6
0+ 0
²³⁸₉₂U
4→2 103.5
6→4 159.4
8→6 211.1
10→8 258.3
12→10 301.2
14→12 339
U K X-ray
NUMBER OF γ-RAYS
E γ (keV)

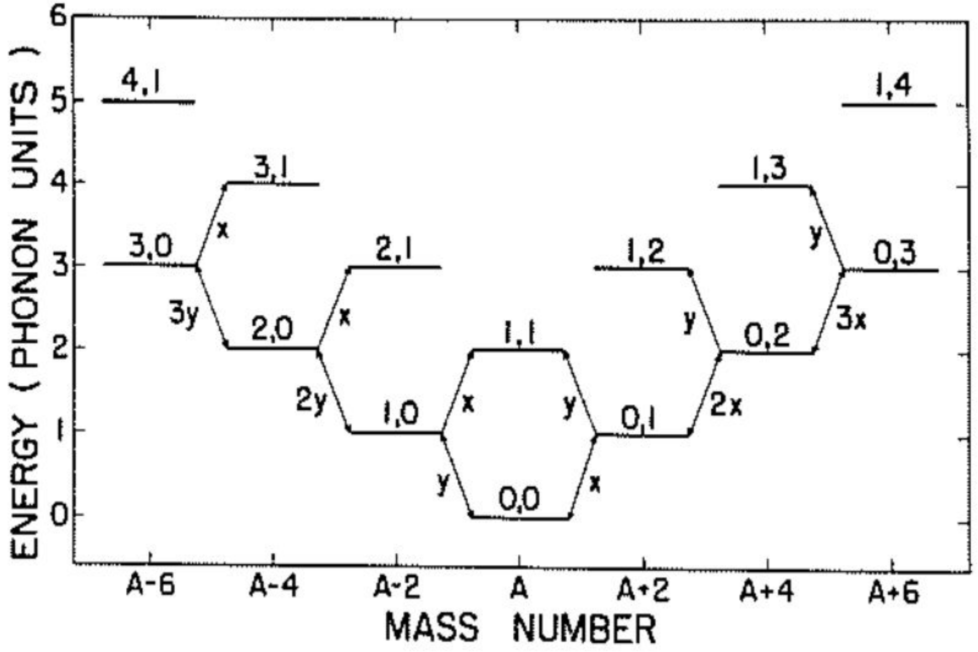

ENERGY (PHONON UNITS)
MASS NUMBER
A-6
A-4
A-2
A
A+2
A+4
A+6
4,1
3,1
3,0
2,1
2,0
1,2
1,3
1,4
0,3
1,1
1,0
0,1
0,2
0,0
x
y
3y
2y
2x
3x

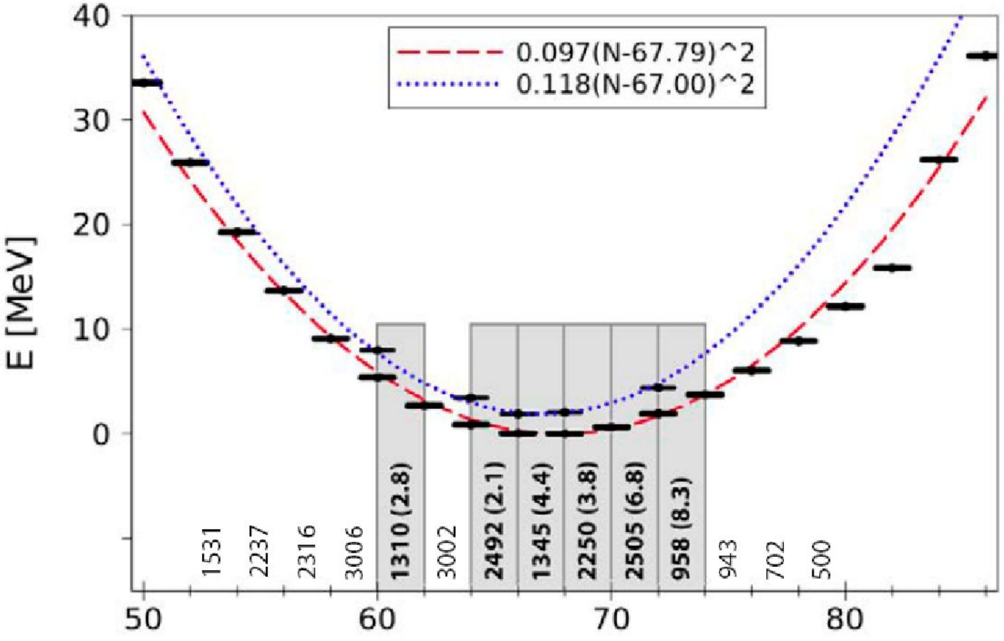

0.097(N-67.79)^2
0.118(N-67.00)^2
E [MeV]
1531
2237
2316
3006
1310 (2.8)
3002
2492 (2.1)
1345 (4.4)
2250 (3.8)
2505 (6.8)
958 (8.3)
943
702
500

The pp-RPA equations

$$|A+2,\tau\rangle = \Big(\sum_{m<n} X^{\tau}_{mn} a^{+}_{m} a^{+}_{n} - \sum_{i<j} Y^{\tau}_{ij} a^{+}_{j} a^{+}_{i} \Big) |A,0\rangle$$

$$\begin{pmatrix} A & B \\ B^{+} & C \end{pmatrix} \begin{bmatrix} R_p^{\tau,\lambda} \\ R_h^{\tau,\lambda} \end{bmatrix} = \begin{pmatrix} 1 & 0 \\ 0 & -1 \end{pmatrix} \begin{bmatrix} R_p^{\tau,\lambda} \\ R_h^{\tau,\lambda} \end{bmatrix} \cdot \hbar\Omega_{\tau,\lambda},$$

$$A_{mnm'n'} = \delta_{mm'}\delta_{nn'}(\epsilon_m + \epsilon_n) + \bar{v}_{mnm'n'},$$

$$C_{iji'j'} = -\delta_{ii'}\delta_{jj'}(\epsilon_i + \epsilon_j) + \bar{v}_{iji'j'},$$

$$B_{mnij} = -\bar{v}_{mnij},$$

$$(R_p^{\tau})_{mn} = X^{\tau}_{mn}, \qquad (R_p^{\lambda})_{mn} = Y^{\lambda}_{mn},$$

$$(R_h^{\tau})_{ij} = Y^{\tau}_{ij}, \qquad (R_h^{\lambda})_{ij} = X^{\lambda}_{ij}.$$

Vmnm'n' = 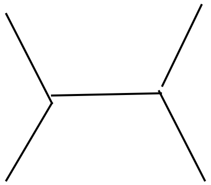

Viji'j' = 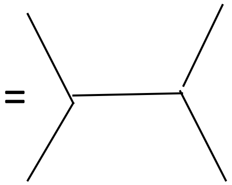

Vmnij = 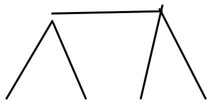

Tne Nuclear Many Body Problem
Ring and Schuck

Mixing and GSC

$X_{mn}(r) =$

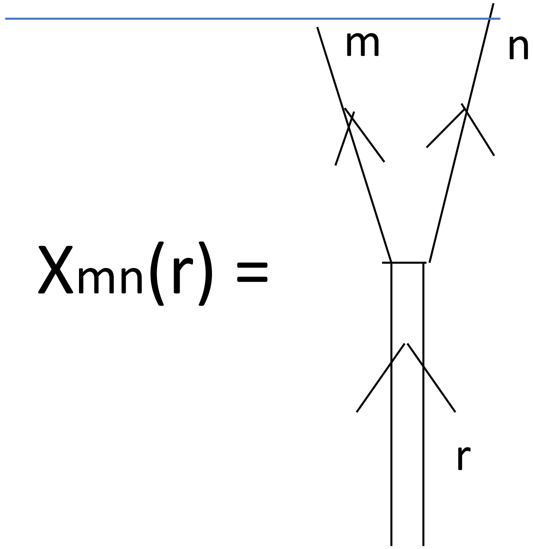

$Y_{ij}(r) =$

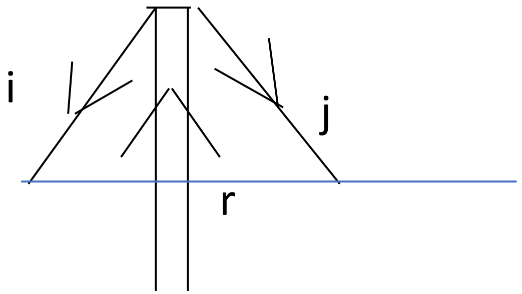

Several unsuccessful experimental searches have been carried out over the years , but recently a bump has been detected at E* ≈ 16 MeV in the reaction $^{12}C(^{18}O,^{16}O)^{14}C$ at E_{lab} = 84 and 275 MeV and intepreted as a signature of GPV

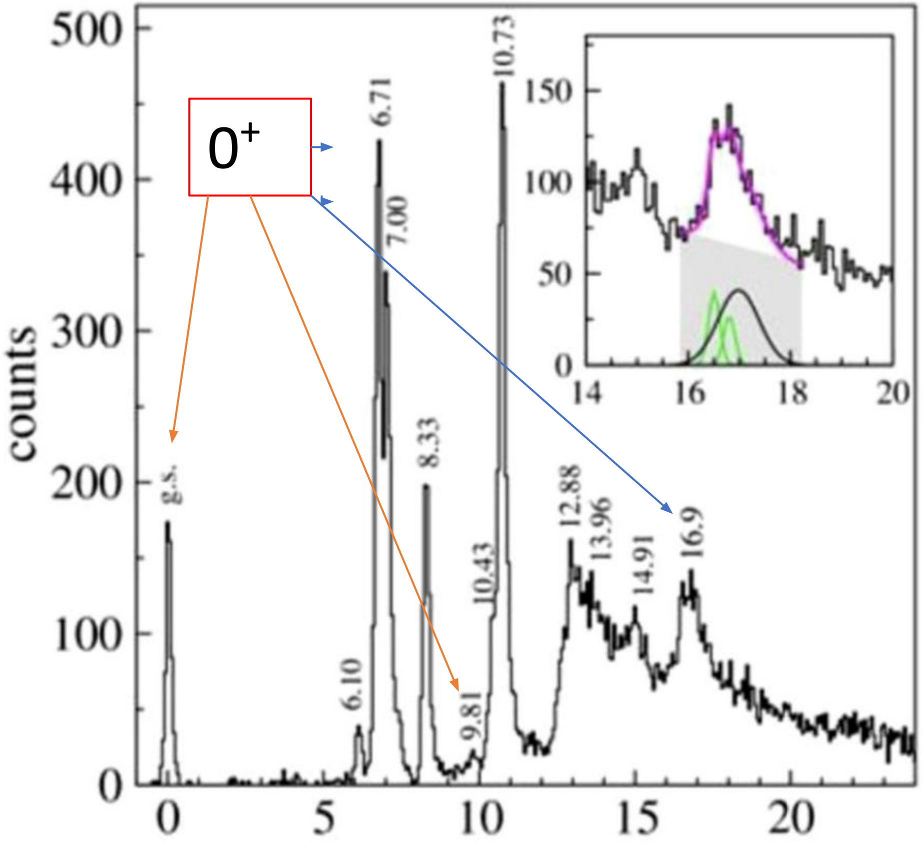

F. Cappuzzello et al., Nat. Comm. 6 (2015) 6743

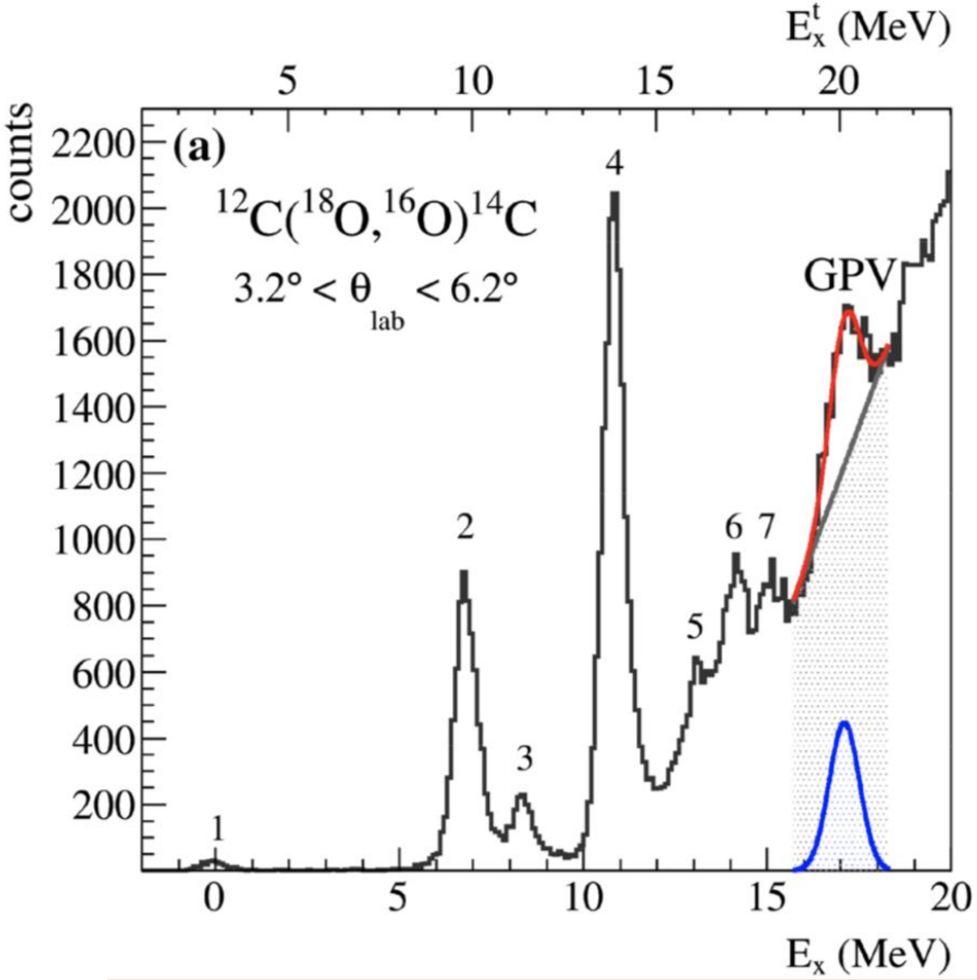

F. Cappuzzello et al., Eur. Phys. J. A 57 (2021) 34

E_{lab} = 84 MeV

E_{lab} = 275 MeV

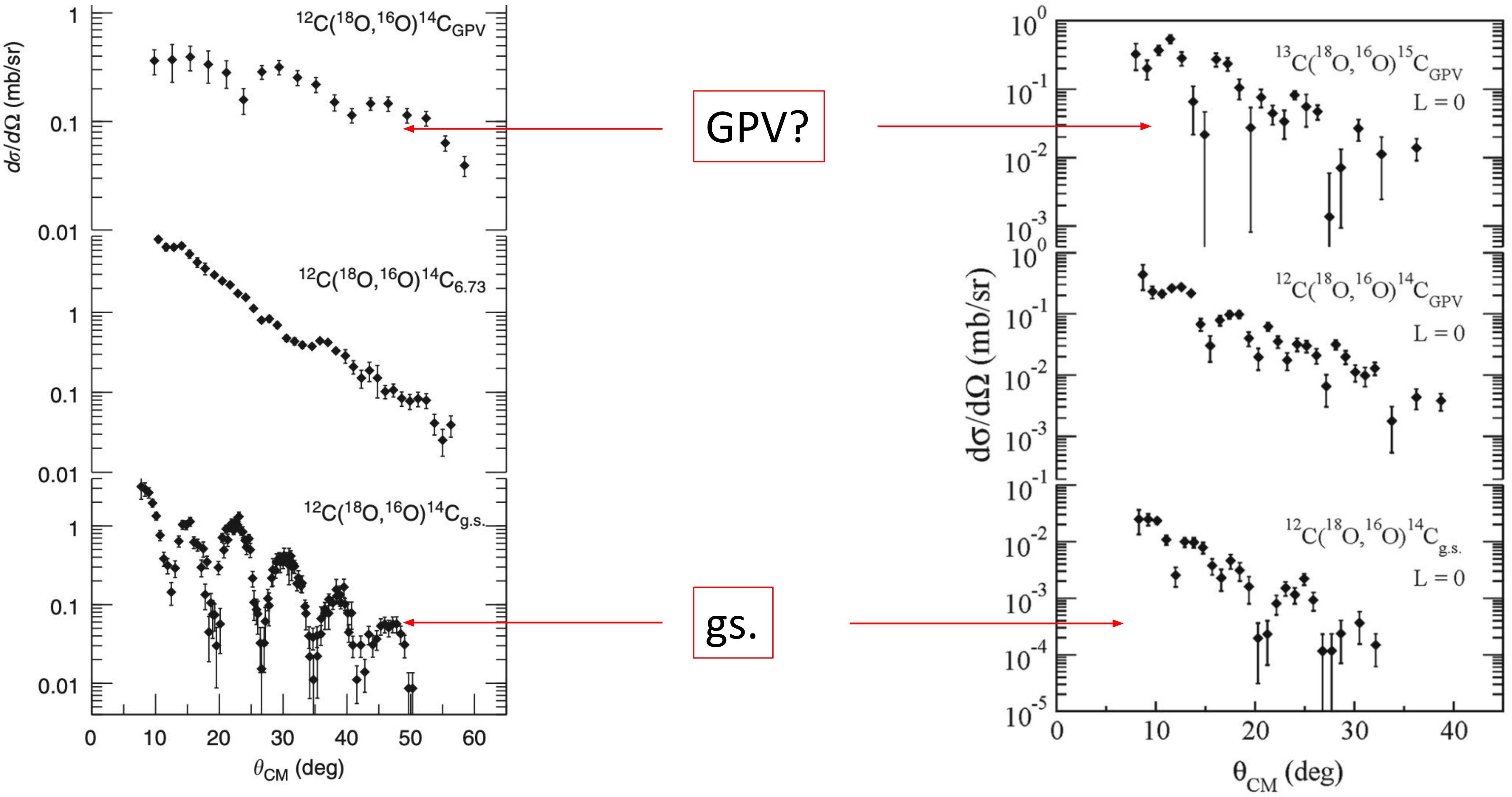

^{16}O

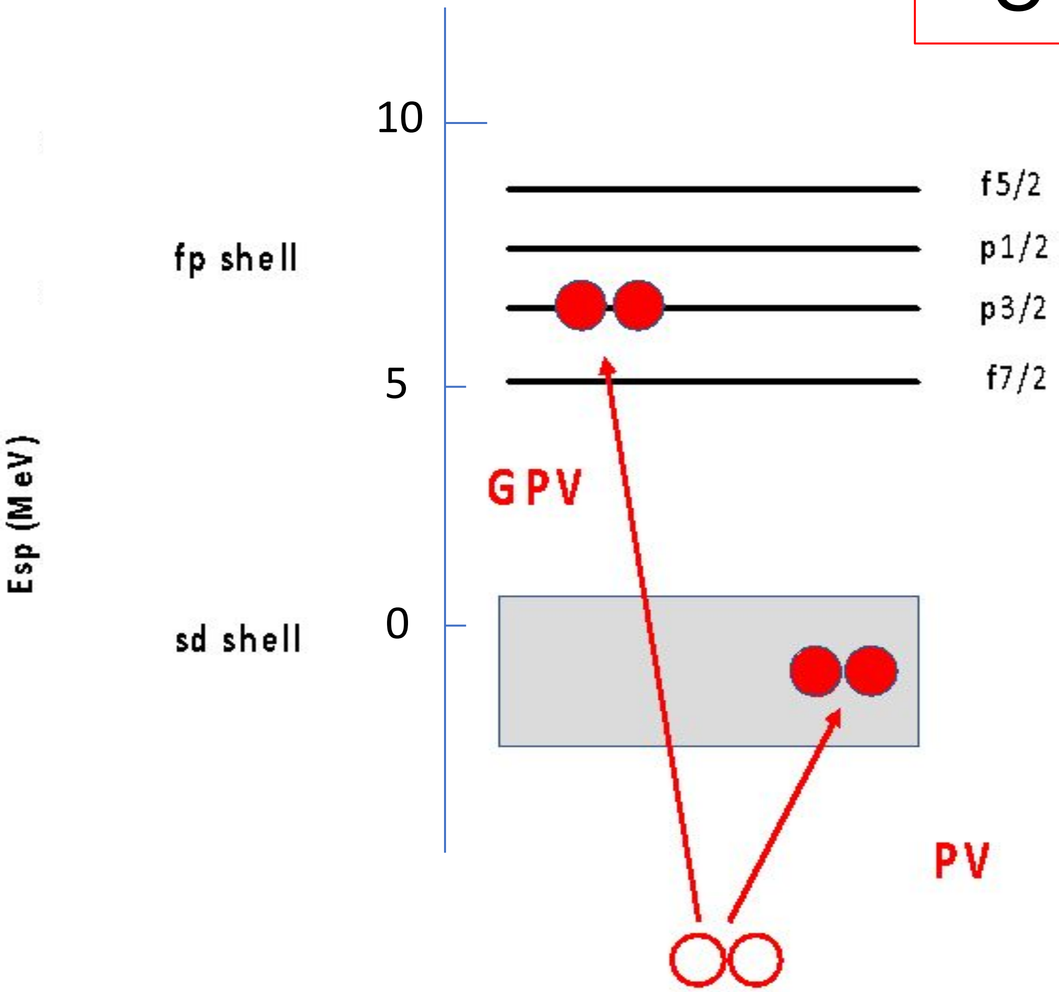

In the GPV both neutrons lie in the continuum

This brings some complications:

We will use Reflecting Spherical Box boundary conditions for discretizing continuum ppRPA using BOX boundary conditions

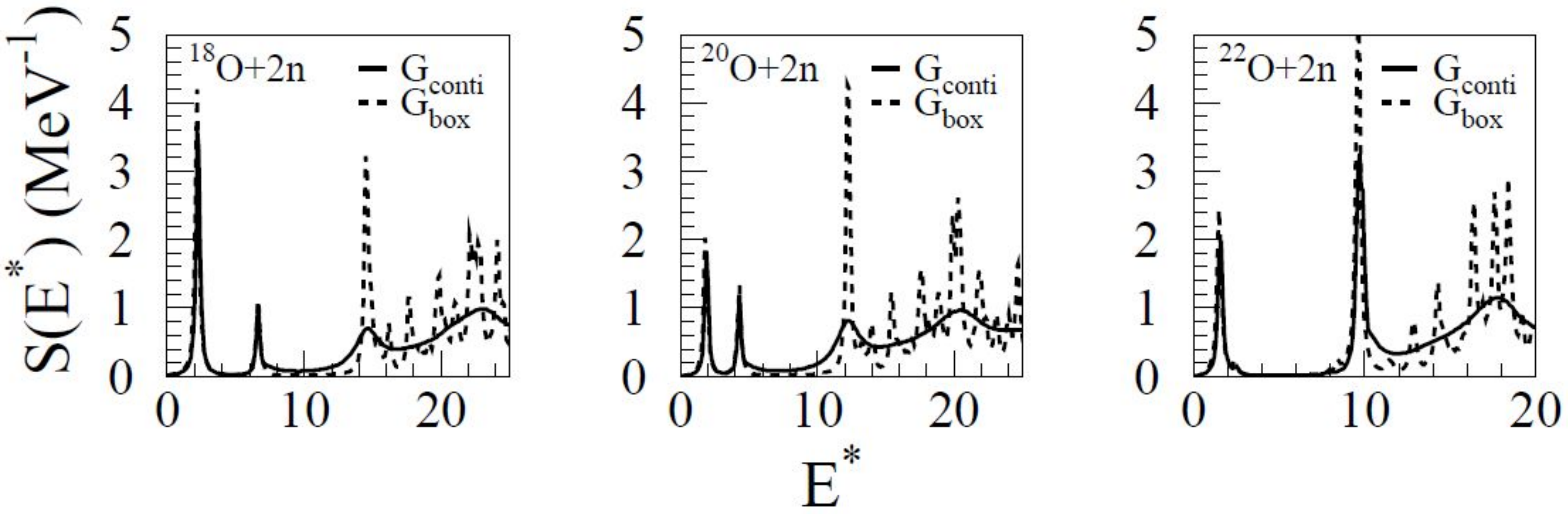

FIG. 1. The QRPA response for the two-neutron transfer on ^{18,20,22}O. The exact continuum calculations are in solid lines whereas the calculations with box boundary conditions are in dashed lines. The results are displayed as functions of E*, the excitation energy with respect to the parent nucleus ground state. Rbox = 22.5 fm

E. Khan et al PRC69 (2004) 014314

Our Continuum Treatment

*Continuum is **discretized** using the s-p states generated within **a set of reflecting spherical boxes of large radii**

$$R_o\,; \quad R_1 = R_o + \Delta R\,; \quad R_2 = R_o + 2\,\Delta R\,;\ldots\ldots \quad R_n = R_o + N\,\Delta R$$

with $R_o \gg R_{nucleus}$,

$\Delta R \ll R_o$,

and N such that $e2(R_N) = e1(R_o)$ (see next slide)

*For **each box-radius** the equations are solved. The final observables (differential cross sections) results are obtained **averaging over/superposition of the different boxes**:

$$\langle S(E,\vartheta)\rangle = \Sigma_{i=0,N}\ S(E,\vartheta;R_i;\Gamma)\ /\ (N+1)$$

(Γ:small smoothing parameter)

*Stability of the final result against R_o and ΔR is required.

Schematics of the averaging procedure

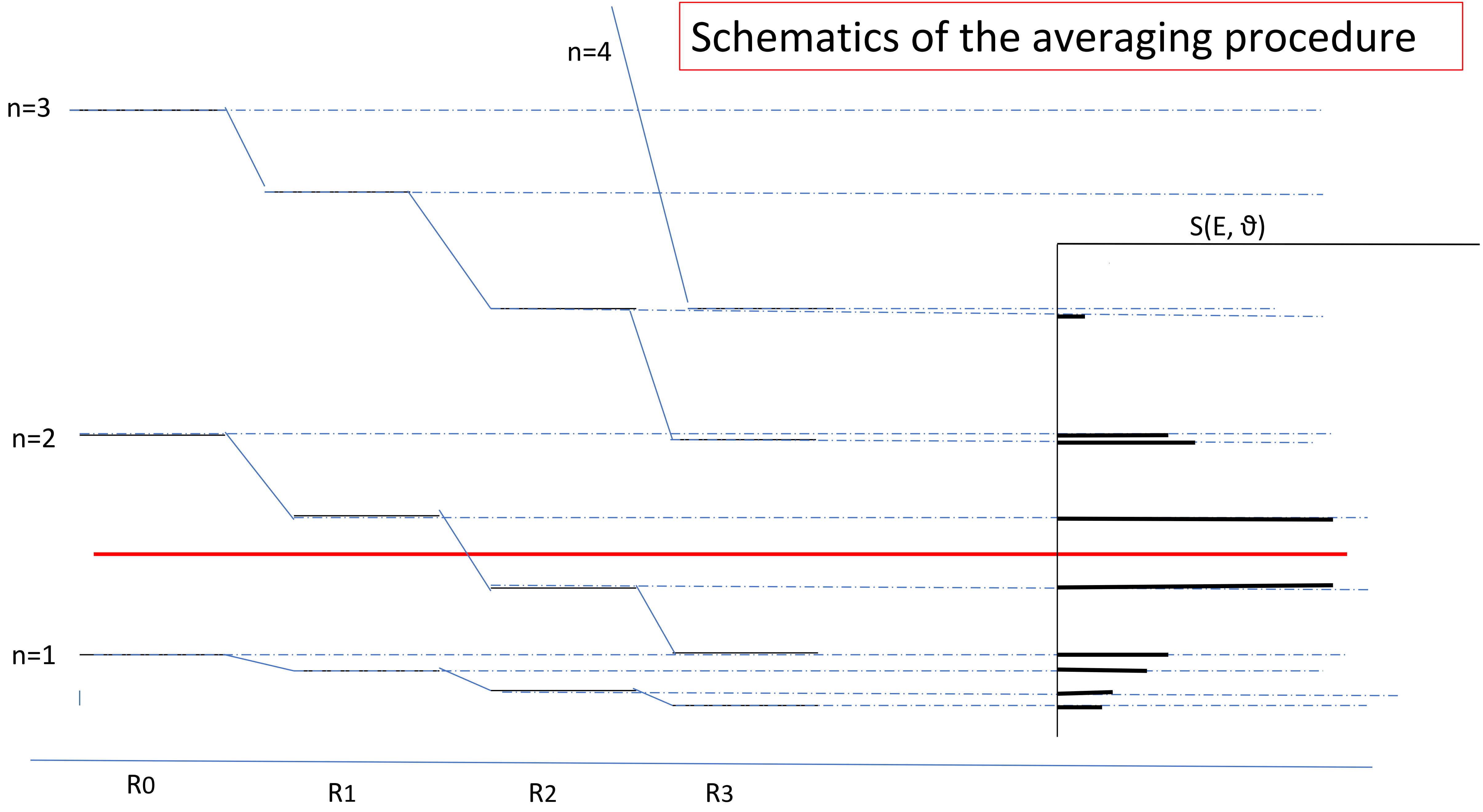

Mixing, GSC and decay width

$X_{mn}(r) =$

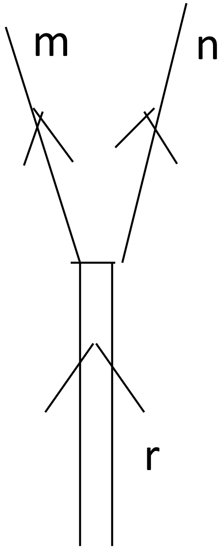

$Y_{ij}(r) =$

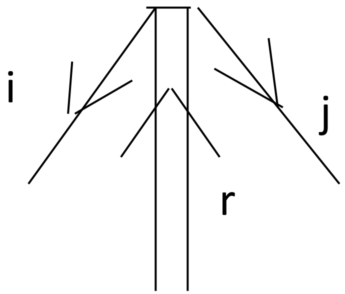

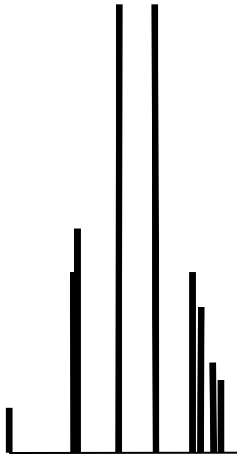

Finally a lorentzian smootning is performed pp-RPA with Sly4 + Gogny(pairing) force

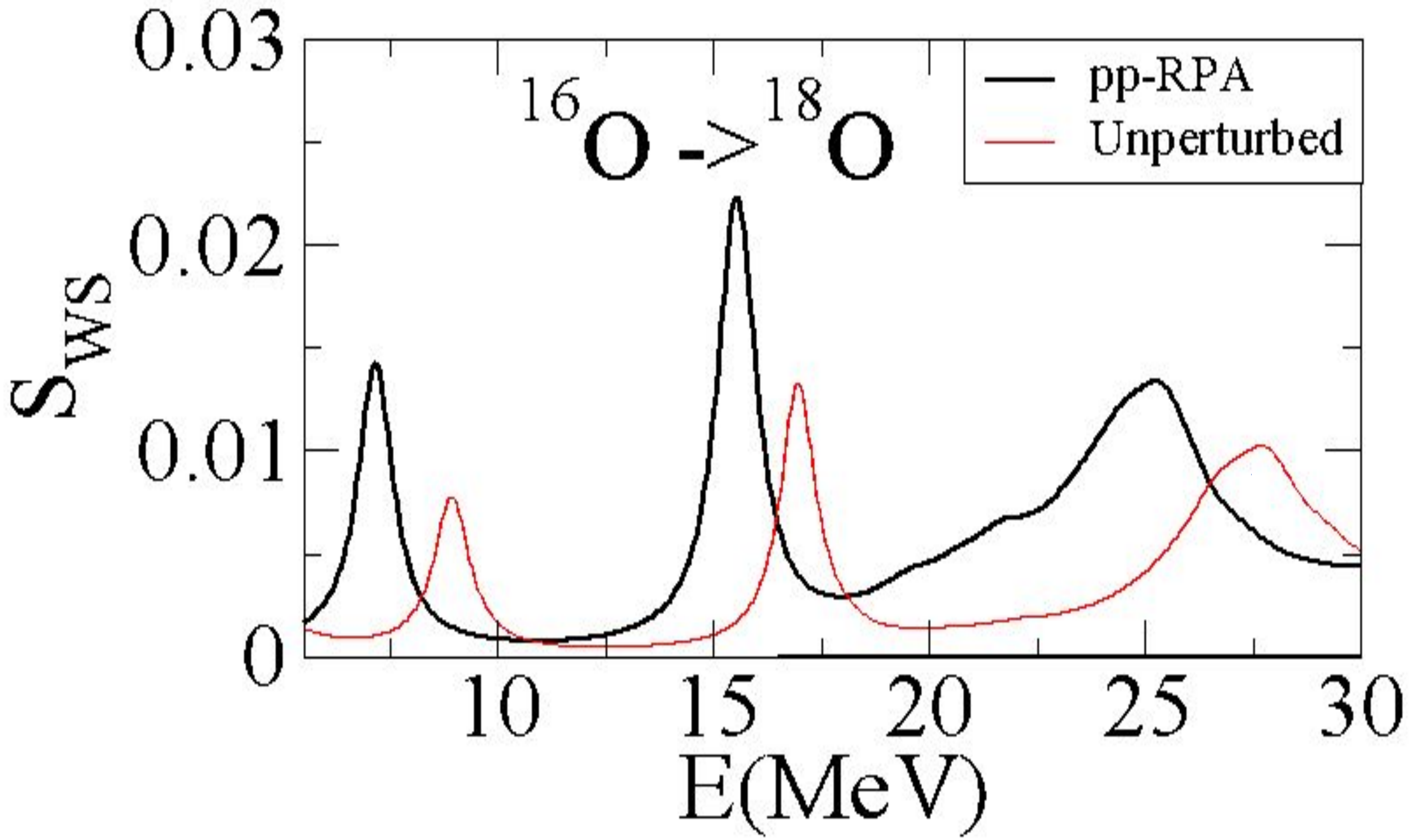

$$S^i_{WS} = \sum_{nn'lj} [X^i_{nn'lj} + Y^i_{nn'lj}] \int dr G(r) \psi_{nlj}(r) \psi_{n'lj}(r).$$

$$G(r) \equiv (1 + exp[(r - R_S)/a_S]$$

pp-RPA with the Gogny(pairing) force; Averaging details

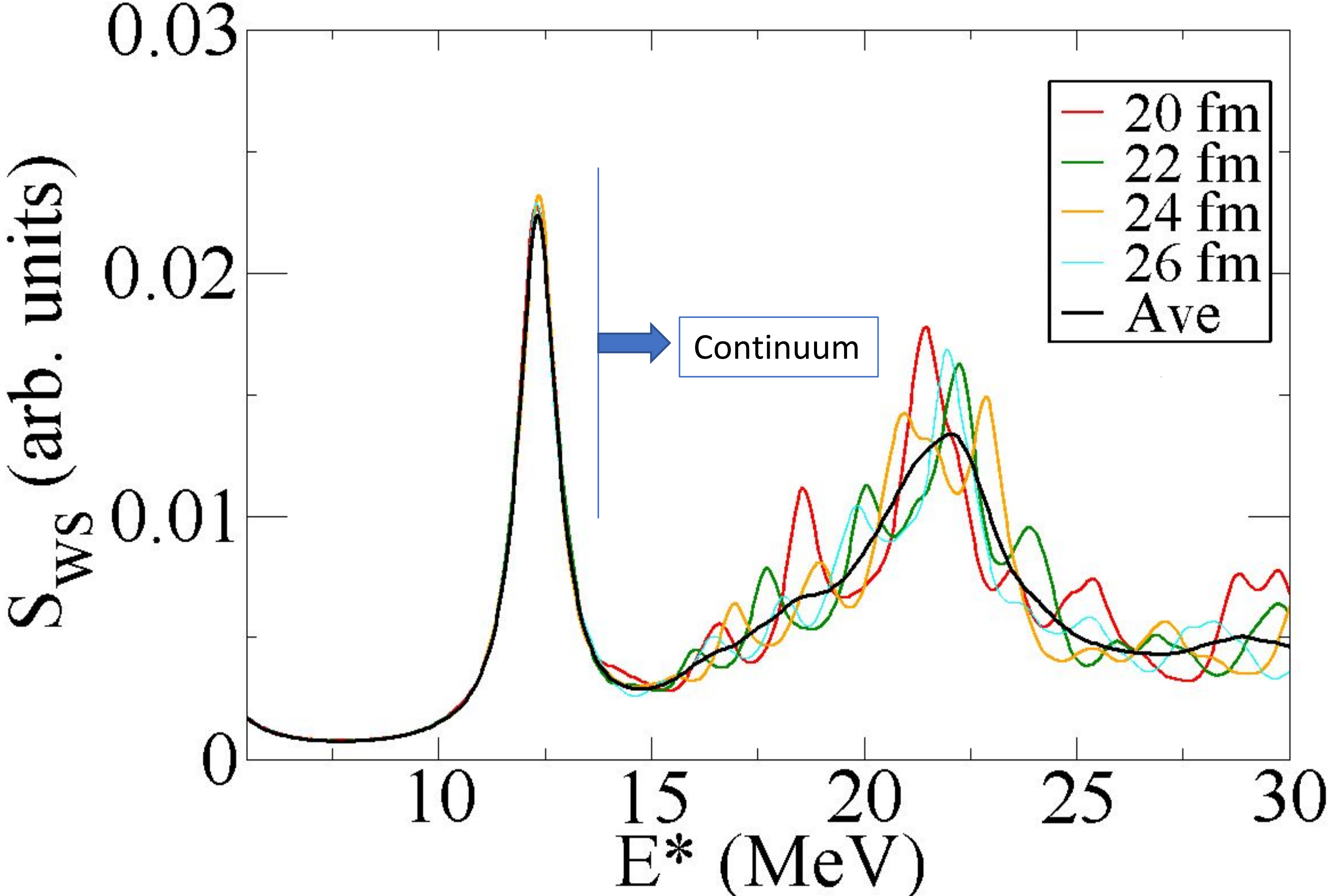

pp-RPA; Comparison with TDHF

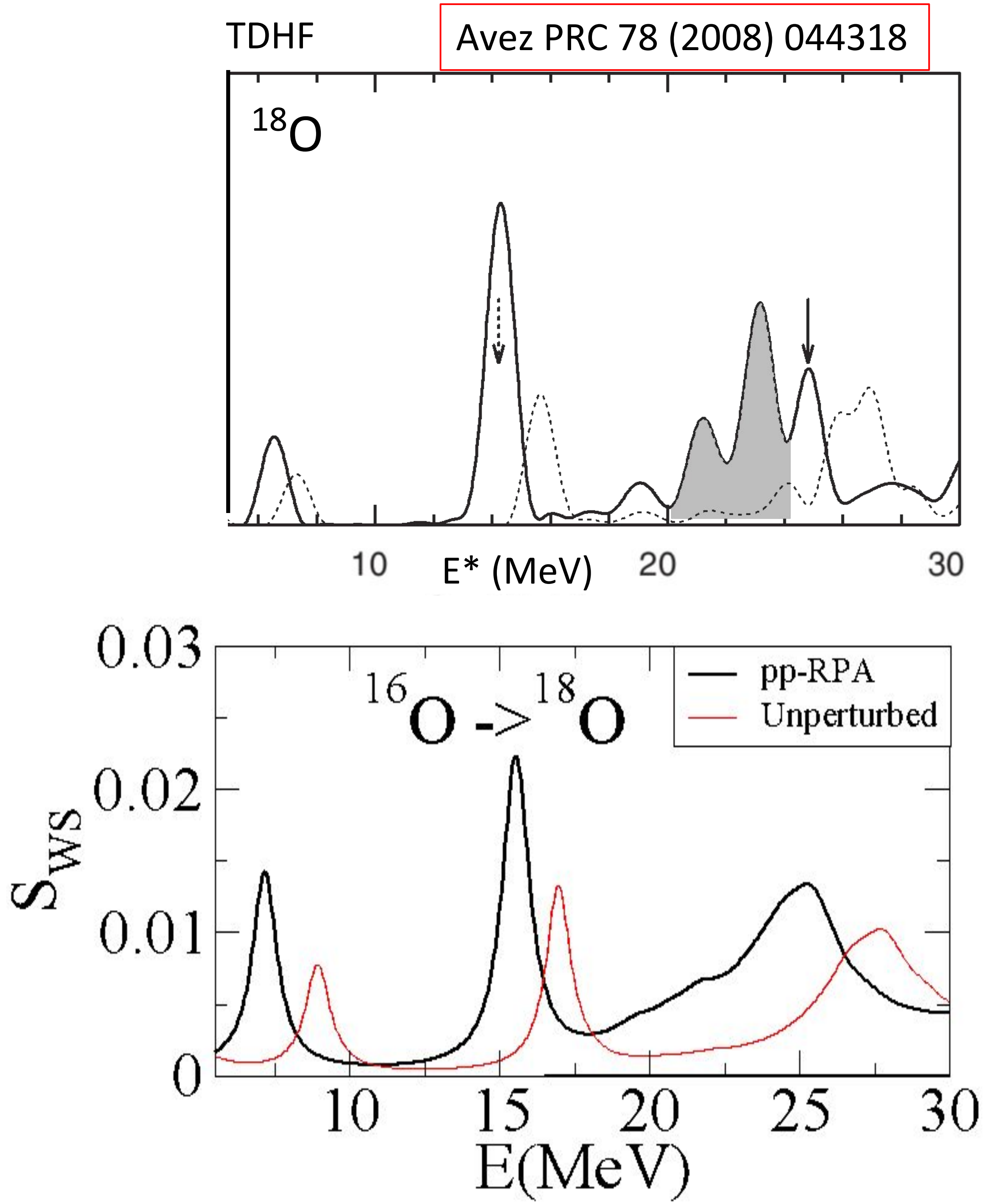

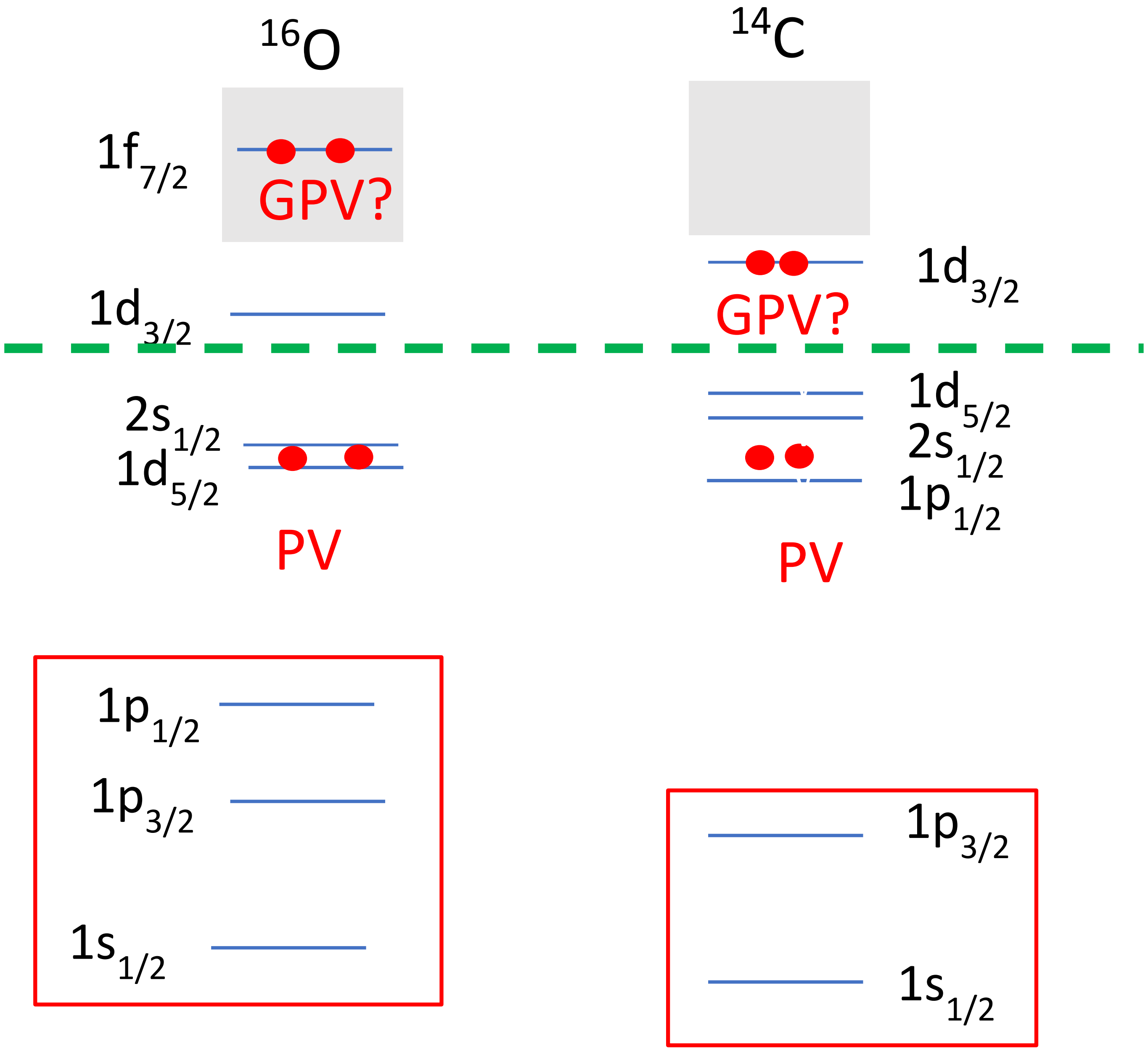

^{16}O
^{14}C
$1f_{7/2}$
GPV?
$1d_{3/2}$
GPV?
$1d_{3/2}$
$2s_{1/2}$
$1d_{5/2}$
$1d_{5/2}$
$2s_{1/2}$
$1p_{1/2}$
PV
PV
$1p_{1/2}$
$1p_{3/2}$
$1s_{1/2}$
$1p_{3/2}$
$1s_{1/2}$

Position of the Single Particle Levels and PVC

Self-energy

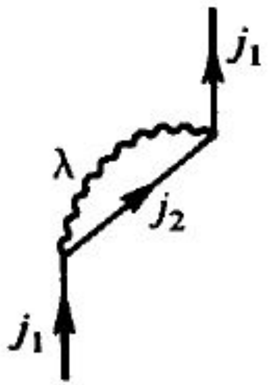

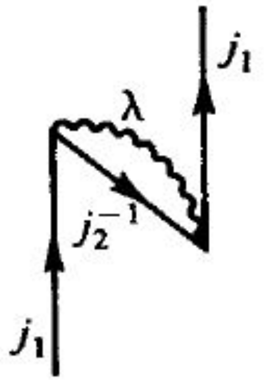

$$\delta\varepsilon(j_1) = \begin{cases} \dfrac{h^2(j_1, j_2\lambda)}{\varepsilon(j_1) - \varepsilon(j_2) - \hbar\omega_\lambda} & \varepsilon(j_2) > \varepsilon_F \\[2ex] -\dfrac{h^2(j_1, j_2\lambda)}{\varepsilon(j_2) - \varepsilon(j_1) - \hbar\omega_\lambda} & \varepsilon(j_2) < \varepsilon_F \end{cases}$$

λ^π: 2^+ most relevant

Part of the S-P strength goes to the intermediate state-> Fragmentation/Width through doorway states

NFT/PVC basic ingredients

Large variety of applications

Vertices

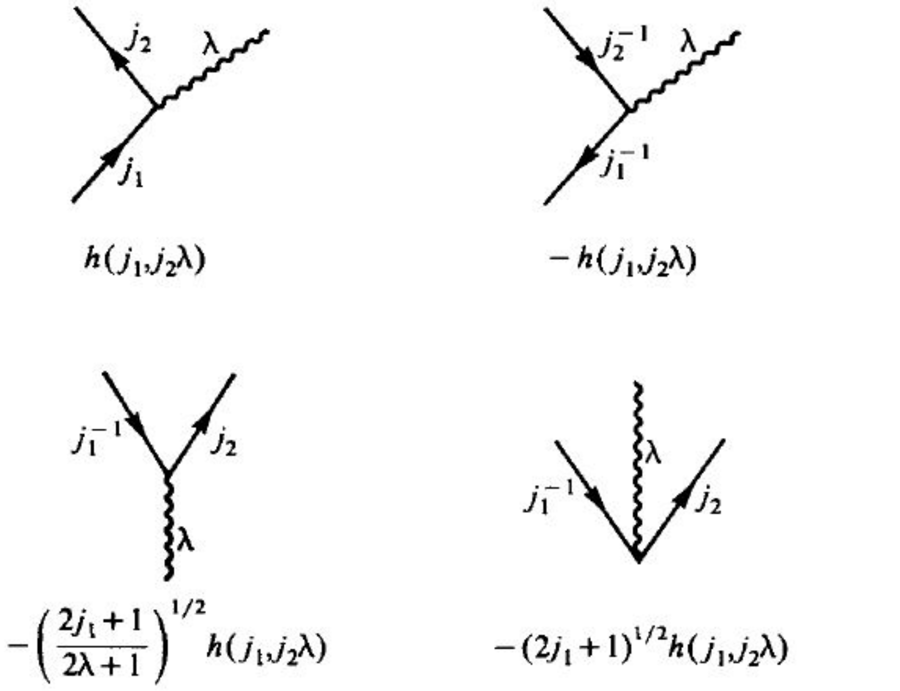

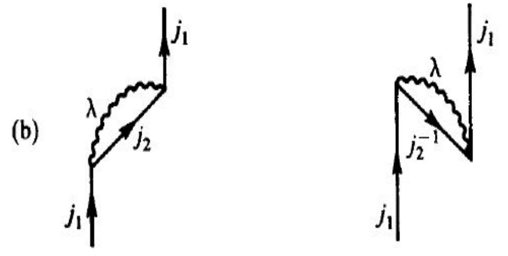

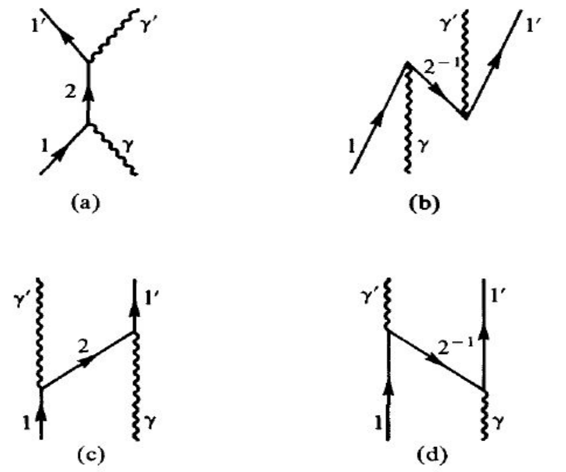

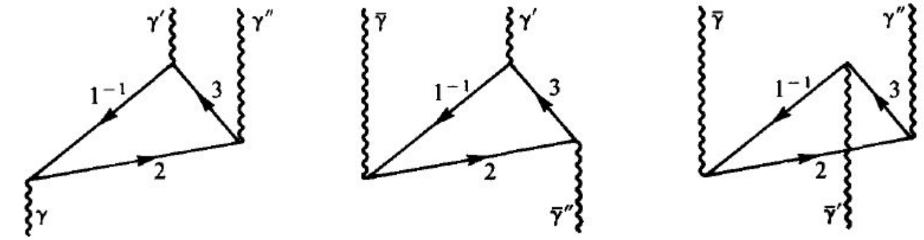

$$h(j_1,j_2\lambda) \equiv \langle j_2, n_\lambda = 1; I = j_1, M = m_1 | H' | j_1 m_1 \rangle$$

$$= (-1)^{j_1+j_2}(2j_1+1)^{-1/2}(2\lambda+1)^{-1/2}\langle j_2 \| k_\lambda Y_\lambda \| j_1 \rangle \langle n_\lambda = 1 \| \alpha_\lambda \| n_\lambda = 0 \rangle$$

Many-body states in N=7 isotones arising from quadrupole coupling with single-particle states calculated in a common mean-field potential

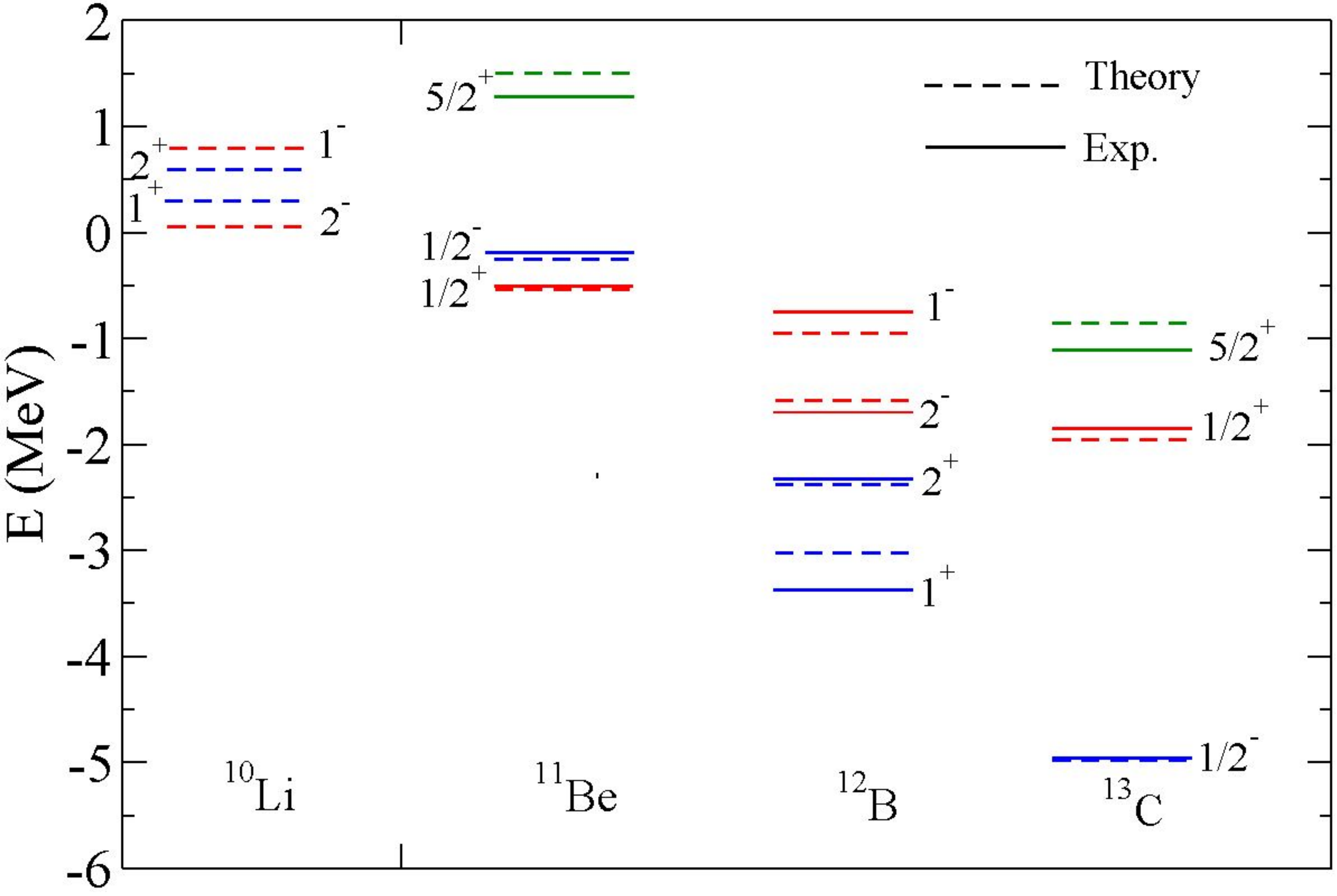

$3/2^+$ many-body phase shift

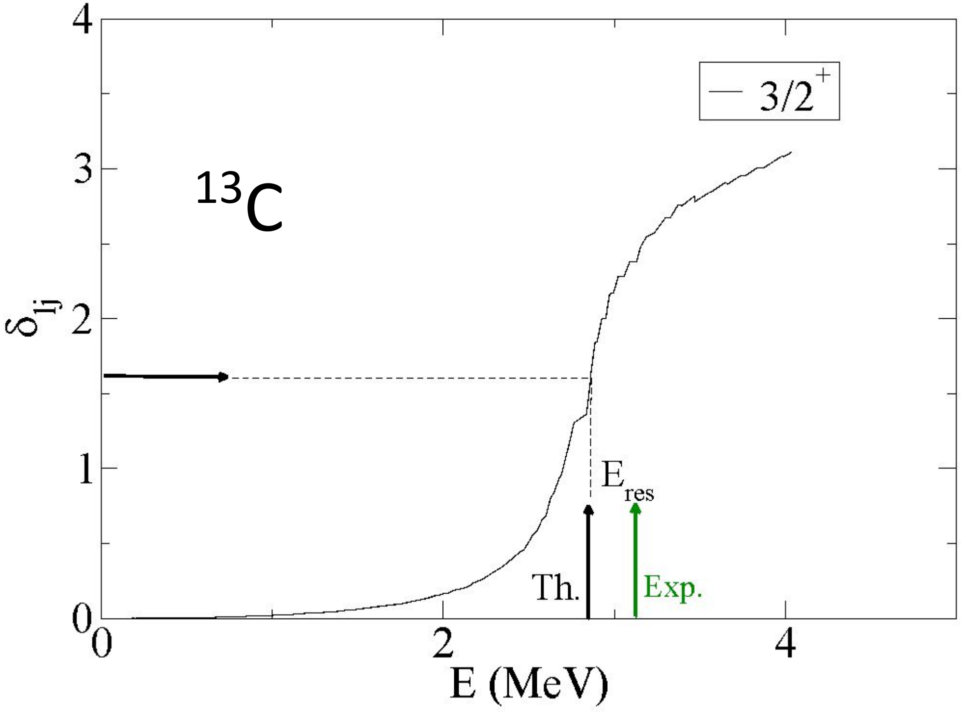

Other data

11Be

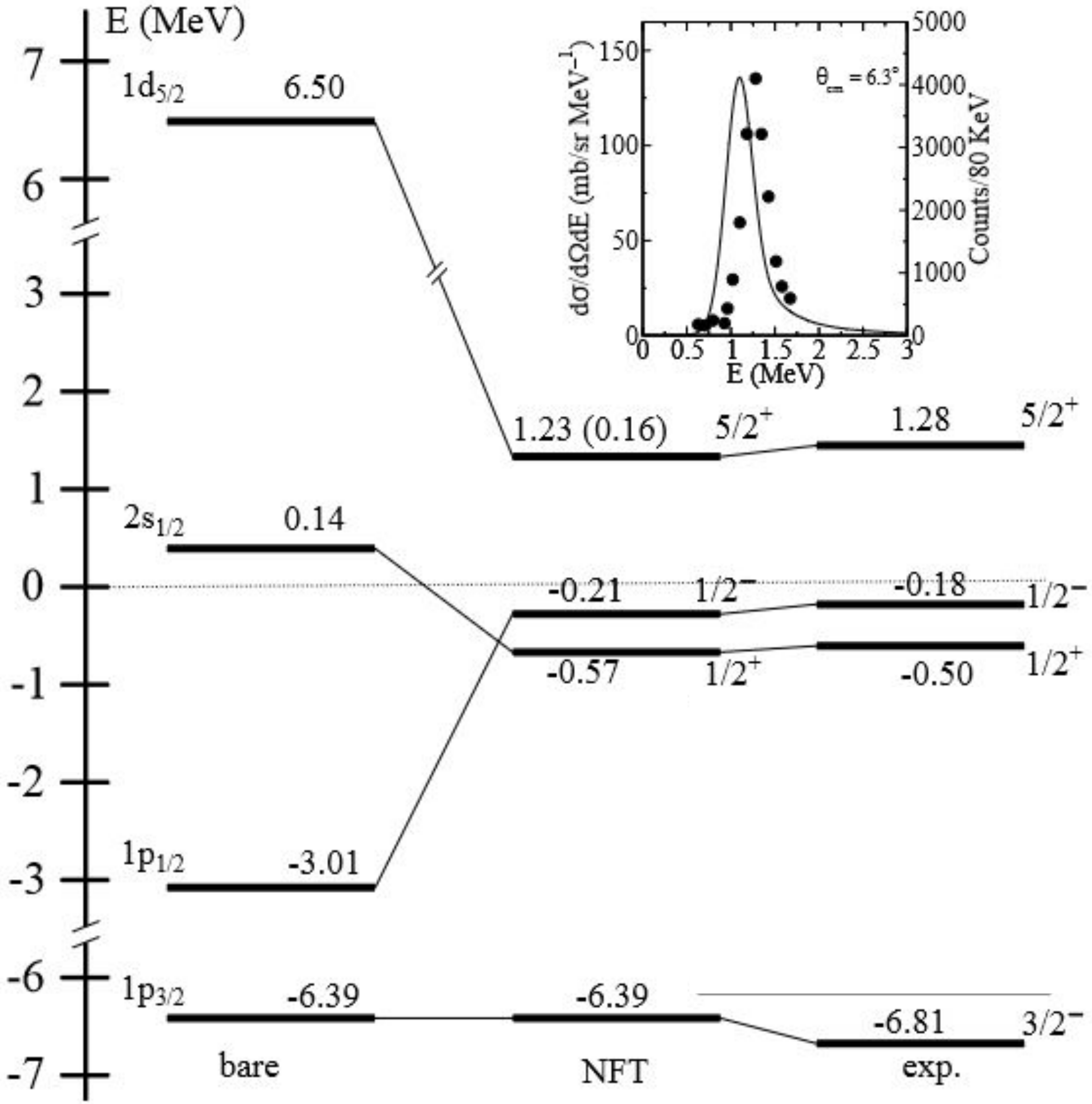

11Be NFT corrections

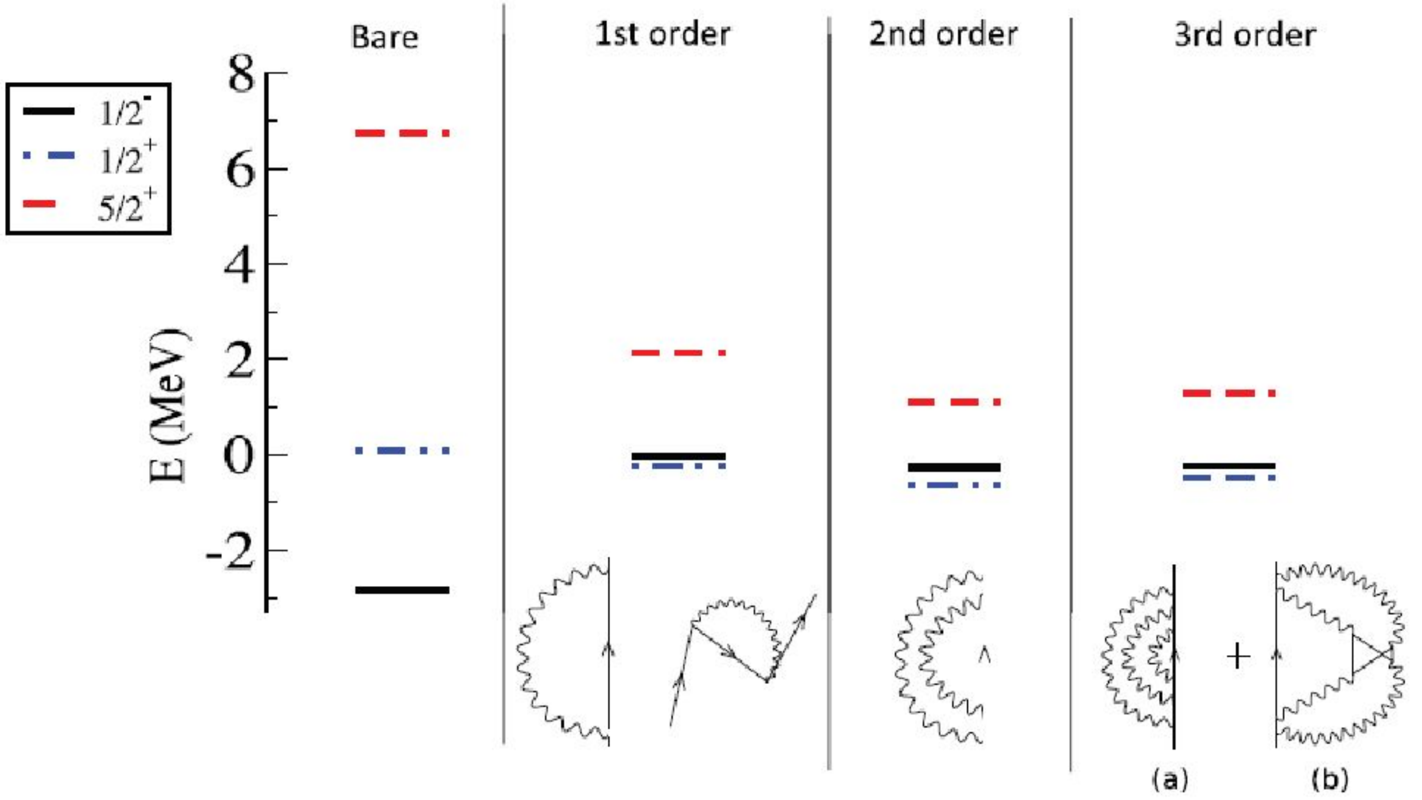

Figure 1. (color online) Theoretical spectrum of low-lying states of ^{11}Be, calculated in different perturbation orders in NFT. The lowest $1/2^-$,$1/2^+$ and $5/2^+$ levels are shown by solid, dot-dashed and dashed lines respectively. In the case of $5/2^+$, the energy of the resonant state is indicated. Representative diagrams included at each order are drawn at the bottom of the figure.

Other data

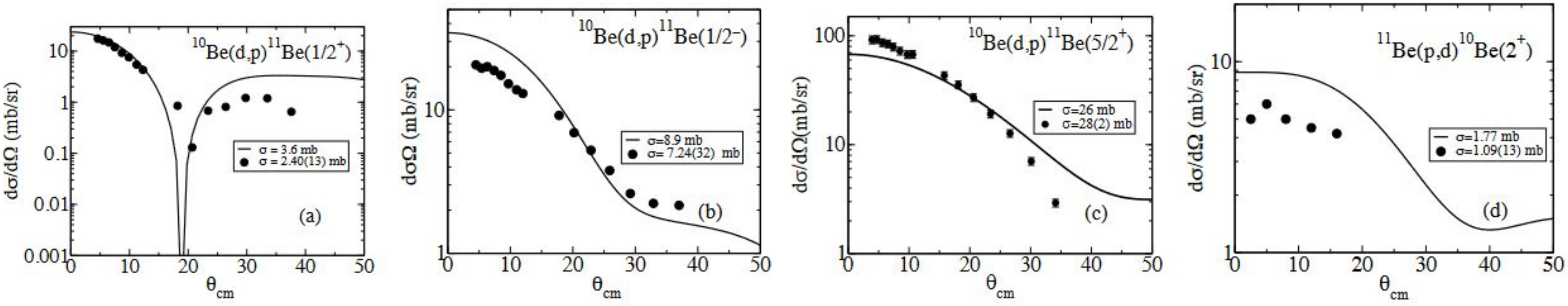

FIG. 4. **(a-c)** (continuous curve) Absolute differential and summed cross sections associated with the reactions ^{10}Be(d,p)^{11}Be, populating the $1/2^+, 1/2^-$, and $5/2^+$ states ($E_d = 21$ MeV). The experimental data [7] are displayed in terms of solid dots. **(d)** Same as before, but for the reaction ^{11}Be(p,d)^{10}Be, populating the 2^+ state ($E_p = 35.3$ MeV/n) [4].

F. Barranco et al, PRL 119 (2017) 082501

Bare mean field potential for N=7 isotones

	$\hbar\omega_{2^+}$ (MeV)	β_2^n	V_{WS} (MeV)	V_{ls}	a_{WS} (fm)	R_{WS} (fm)
^{10}Li	3.37	0.68	64.0	0.50	0.75	2.10
^{11}Be	3.37	0.71	72.0 (73.8)	0.58 (0.54)	0.72 (0.78)	2.14
^{12}B	3.80	0.57	76.8	0.65	0.78 (0.76)	2.18
^{13}C	4.4	0.46(0.43)	82(83.0)	0.76(0.7)	0.73 (0.72)	2.23 (2.25)

New simple parametrization:

V_{WS}=-82+54(N-Z)/A *MeV*
a = 0.75 *fm;* R_{WS}=0.99$A^{1/3}$ *fm*
V_{LS}=0.0082V_{WS}

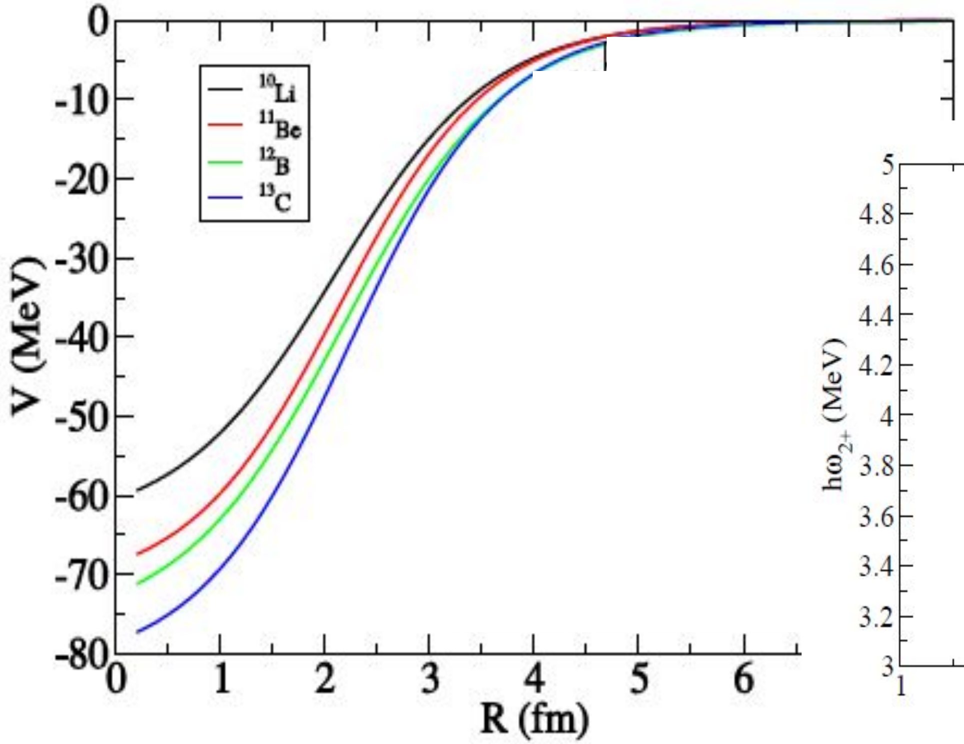

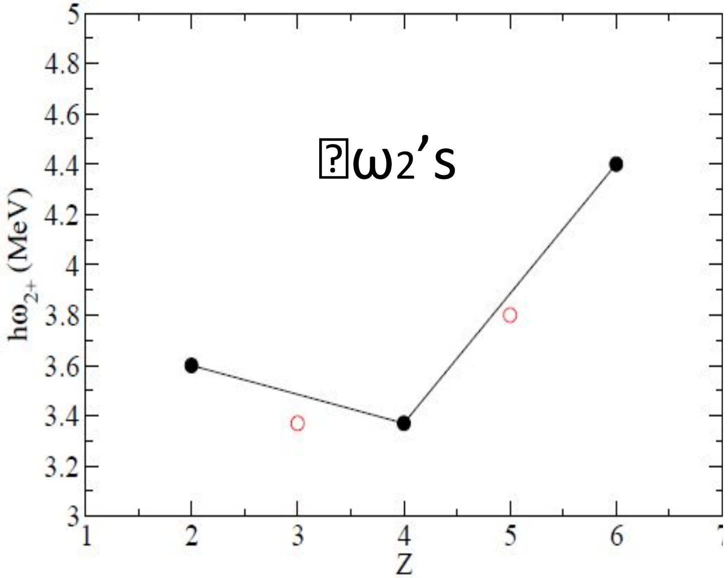

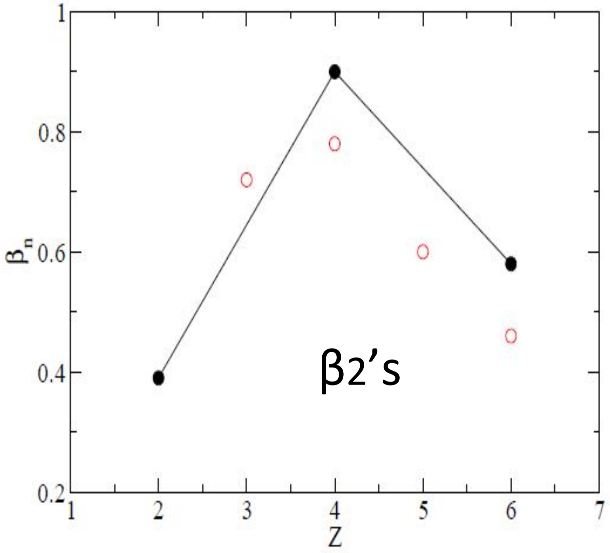

Evidence of phononic components in direct reactions

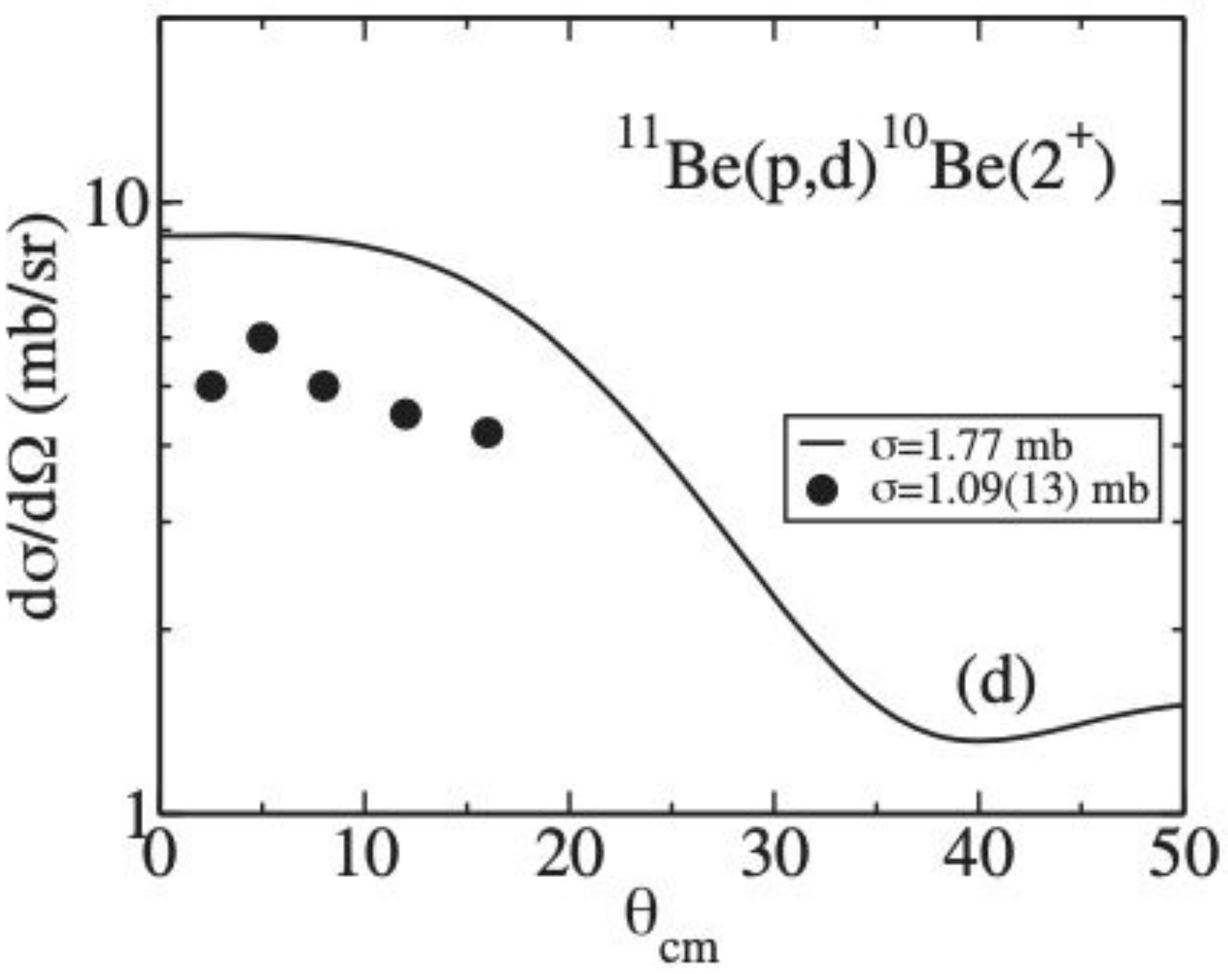

G. Potel et al, PRL 105 (2010) 172502

F. Barranco et al, PRL 119 (2017) 082501

Extended Role of Vibrations in the PV and GPV:

The Phonon Exchange Induced Interaction,

V^{ind}

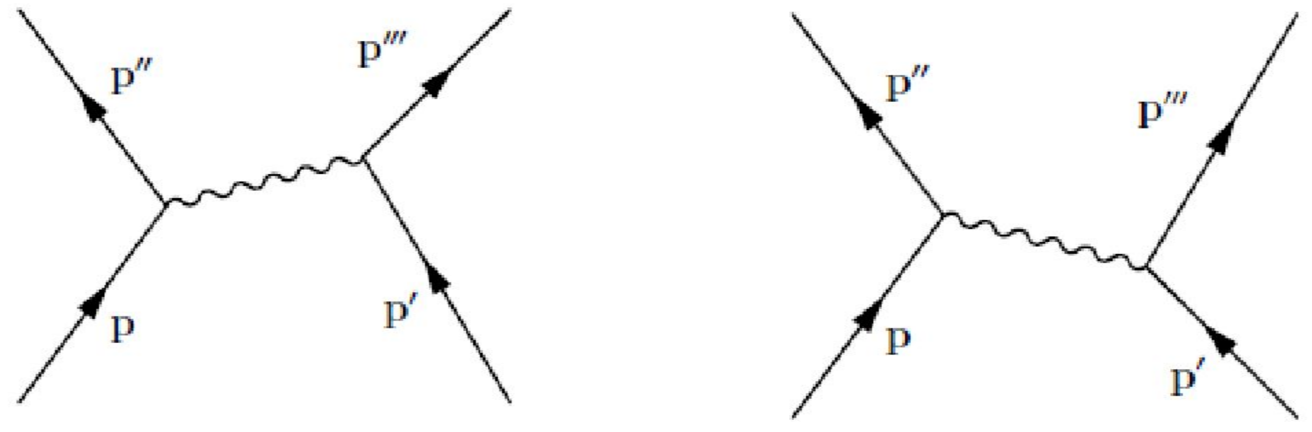

As a consequence: pairing $V^{bare}(p,p';p'',p''')$ must leave room to V^{ind} reduced V^{bare} by 20%

EXTENDED pp-RPA (E-dependent)

$$\begin{pmatrix} A_{pp'p''p'''} & B_{pp'h''h'''} \\ -B_{p''p'''hh'} & -A_{hh'h''h'''} \end{pmatrix} \begin{pmatrix} X_{p''p'''} \\ Y_{h''h'''} \end{pmatrix} = E \begin{pmatrix} X_{pp'} \\ Y_{hh'} \end{pmatrix}$$

PVC

$h_{pp''\lambda\nu}$ =

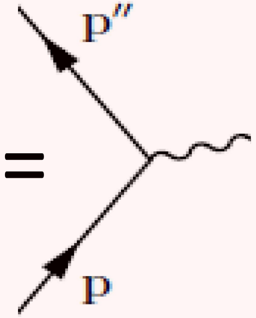

Includes Self-energy and Induced Interaction <-> PVC

$$A_{pp'p''p'''} = [(\epsilon_p + \epsilon_{p'}) + \Sigma_{pp''(p')}(E)\delta_{p'p'''} + \Sigma_{p'p'''(p)}(E)\delta_{pp''} + V^{bare}_{pp'p''p'''} + V^{ind}_{pp'p''p'''}(E) + Exch(p,p')]N_{pp'p''p'''}$$

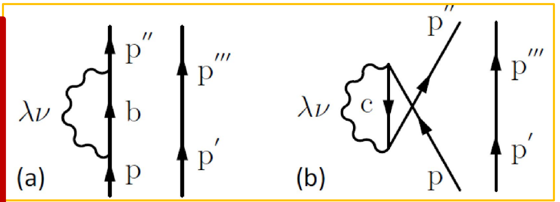

$$B_{pp'hh'} = [V^{bare}_{pp'hh'} + V^{ind}_{pp'hh'}(E) + Exch(p,p')]\, N_{pp'p''p'''}$$

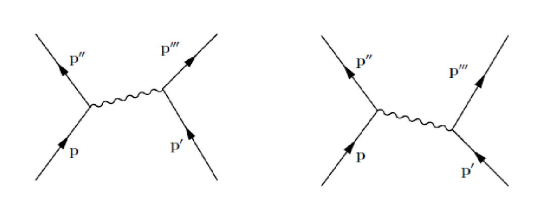

EXTENDED pp-RPA (E-dependent) (detail)

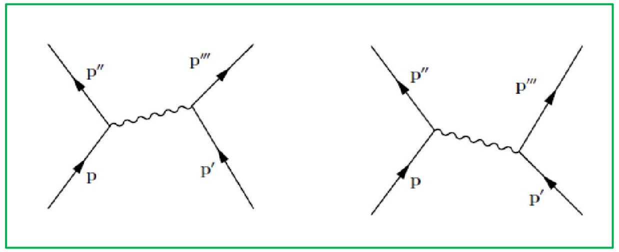

$$V^{ind}_{pp'p''p'''} = \sum_{\lambda\nu}\left[\frac{h_{pp''\lambda\nu}h_{p'''p'\lambda\nu}}{E-(\epsilon^{emp}_{p''}+\epsilon^{emp}_{p'}+\hbar\omega_{\lambda\nu})}+\frac{h_{p''p\lambda\nu}h_{p'p'''\lambda\nu}}{E-(\epsilon^{emp}_{p}+\epsilon^{emp}_{p'''}+\hbar\omega_{\lambda\nu})}\right]$$

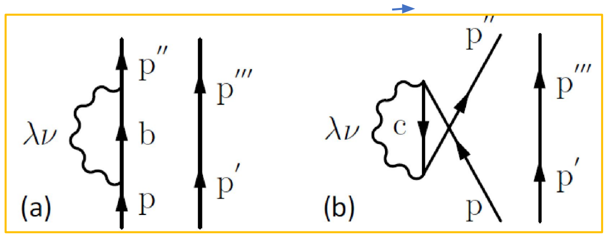

$$\Sigma_{pp''(p')}(E) = \sum_{b,\epsilon_b>\epsilon_F\,\lambda\nu}\frac{h_{pb\lambda\nu}h_{p''b\lambda\nu}}{E-(\epsilon^{emp}_{b}+\epsilon^{emp}_{p'}+\hbar\omega_{\lambda\nu})}+\sum_{c,\epsilon_c<\epsilon_F\,\lambda\nu}\frac{h_{pc\lambda\nu}h_{p''c\lambda\nu}}{E-\epsilon^{emp}_{c}-\epsilon^{emp}_{p'}+\hbar\omega_{\lambda\nu}} \quad (6)$$

1. IMPORTANT: This extended pp-RPA is equivalent to the NFT treatment: In fact, If self-energy and Vind are included perturbatively in a second diagonalisation, the following NFT diagrams for the matrix elements appear:

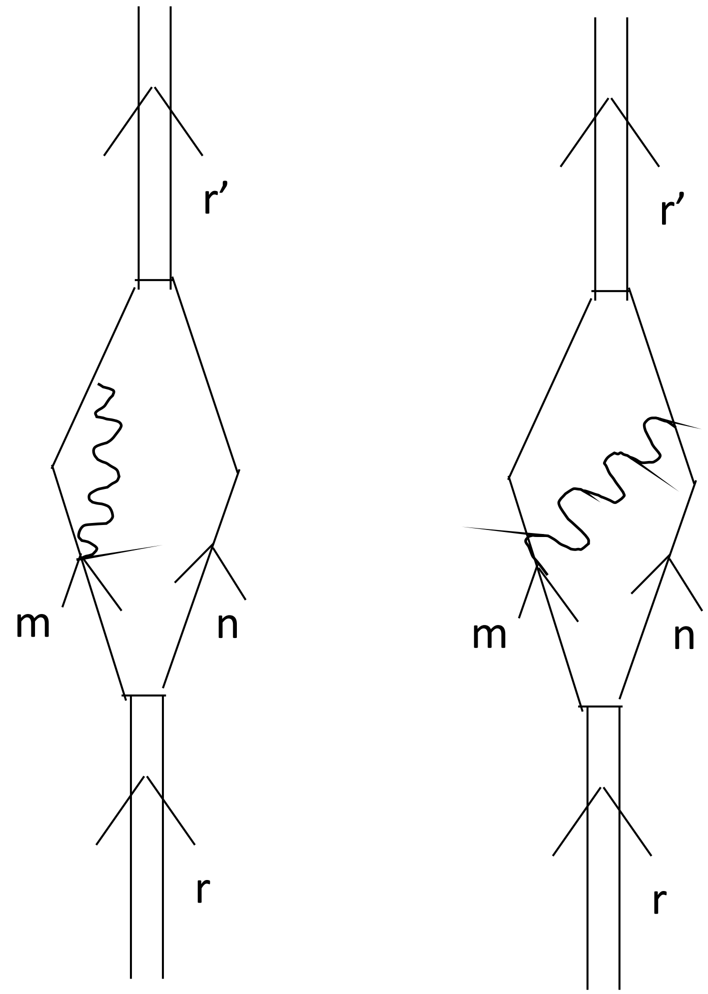

1. The self-energy and the induced interaction are energy-dependent, but it is possible to reconstruct the amplitudes of the resulting 0+ states on the intermediate 2p-1phonon states, so that they can be written:

$$|0^+_n> \;=\; \sum_{pp'} \left(X_{pp'}\ (n)\ |pp'(0^+)> + \ Y_{hh'}\ (n)\ |h\,h'(0^+)> \right) \ +$$
$$\sum_{pp'\nu} R_{pp'\nu}\ (n)\ |pp'(2^+)\nu(2^+)>$$

Role of phononic components in direct reactions

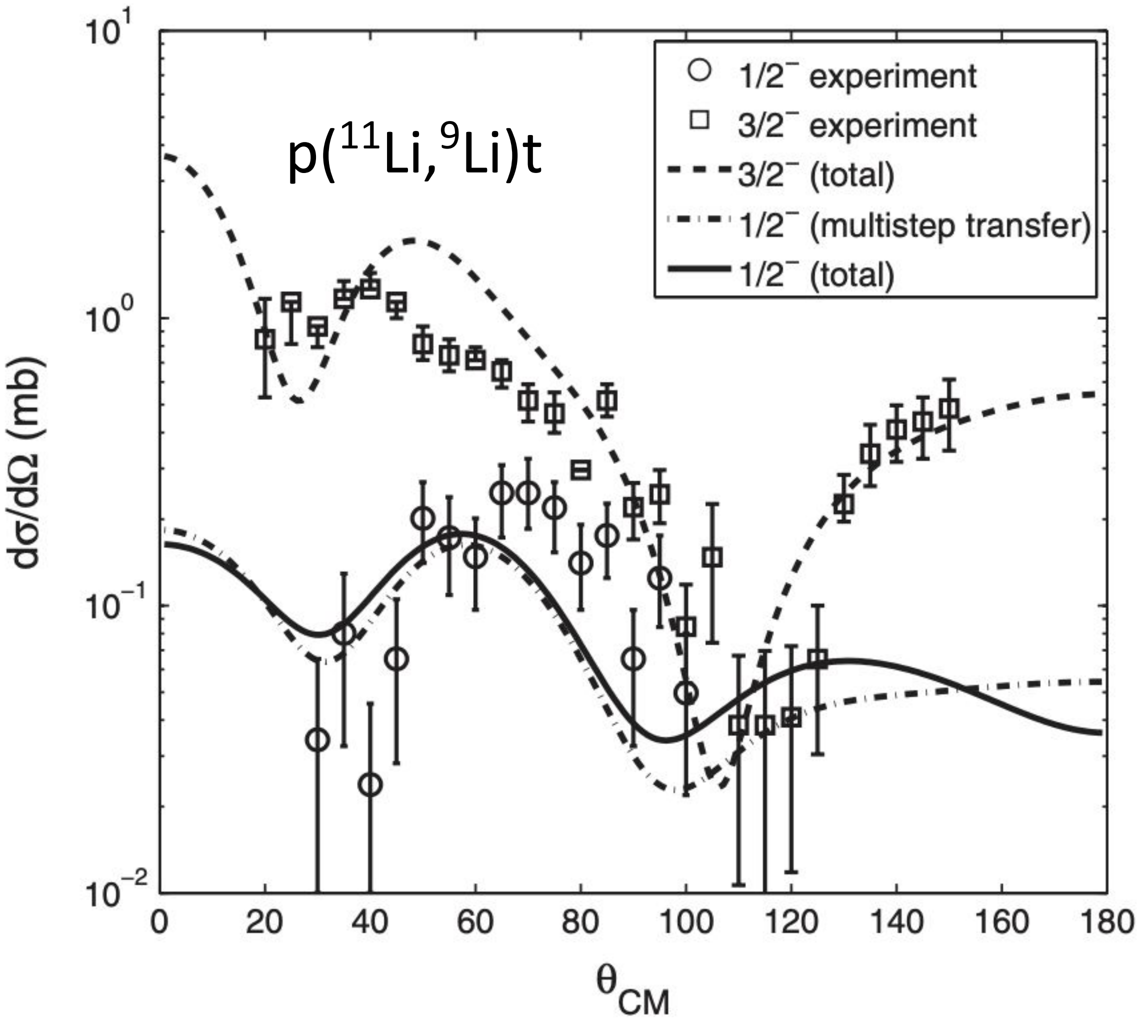

G. Potel et al, PRL 105 (2010) 172502

Mixing, GSC, Decay width and PVC effects

$X_{mn}(r) =$

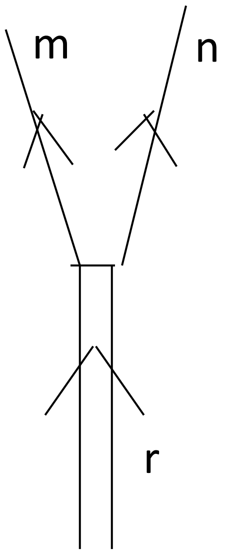

$Y_{ij}(r) =$

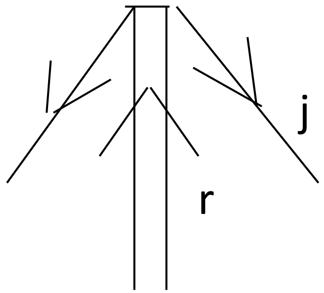

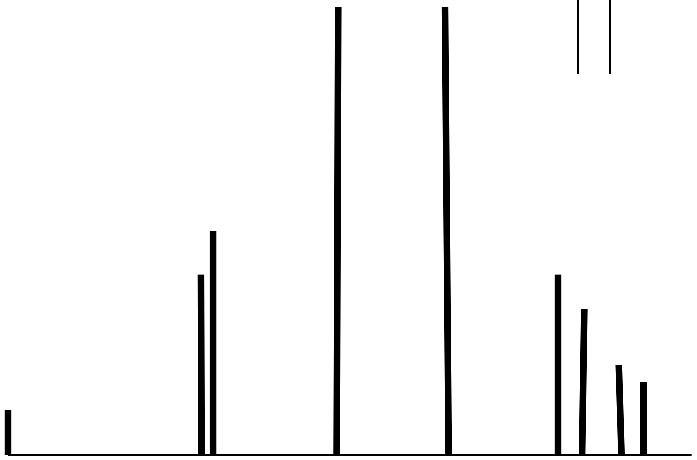

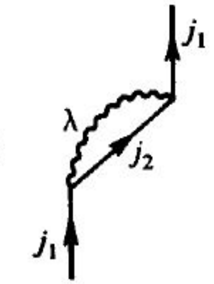

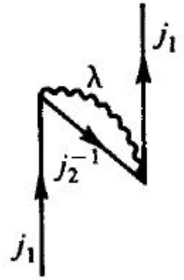

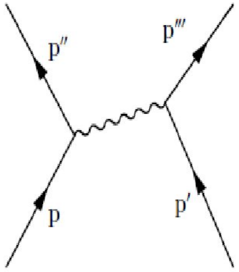

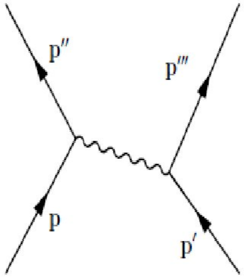

Similar theoretical schemes

Second RPA; Subtraction problem (Exact GS!!)

We (NFT) don't have such constrain

PHYSICAL REVIEW C **92**, 034303 (2015)

Subtraction method in the second random-phase approximation: First applications with a Skyrme energy functional

D. Gambacurta,[1] M. Grasso,[2] and J. Engel[3]

E. Litvinova and Y. Zhang
(arXiv 2208.07843v1; this workshop)

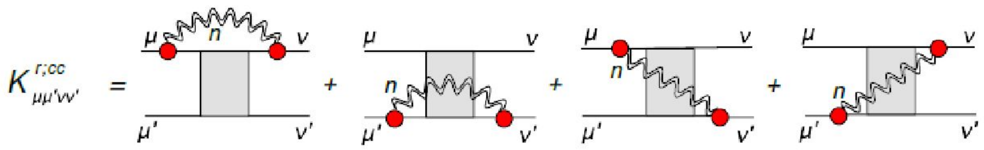

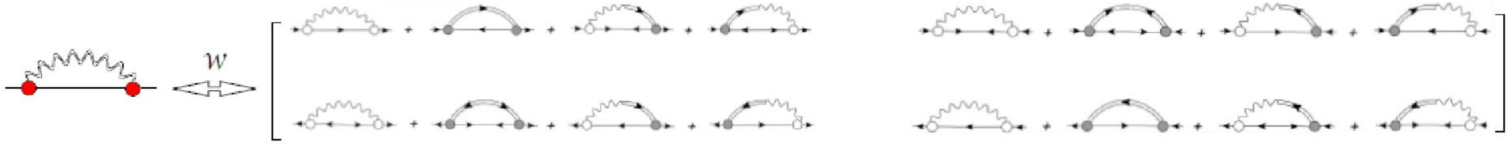

Self Consistent Green Function ("Ab initio" comunity)-? E.Vigezzi's talk for connection with NFT.

Xpp' ; Ypp' and Rpp'2+ amplitudes for 12C + 2n (0+) states: Bound states

	E_{gs}= -13.09 MeV $R^{2_1^+}$ = 0.130			$E_{0_2^+}$= -5.96 MeV $R^{2_1^+}$ = 0.382			$E_{0_3^+}$= -3.47 MeV $R^{2_1^+}$ = 0.348	
l_j	X_{lj}^2	Y_{lj}^2		X_{lj}^2	Y_{lj}^2		X_{lj}^2	Y_{lj}^2
$s_{1/2}$	0.006	0.003		0.283	-		0.376	-
$p_{1/2}$	0.833	-		0.050	-		0.043	-
$p_{3/2}$	-	0.002		0.001	-		-	-
$d_{3/2}$	0.003	-		0.005	-		-	-
$d_{5/2}$	0.046	-		0.327	-		0.256	-

Table 4: Main 0-phonon components of the wavefunctions of the ground state and of the two lowest excited 0^+ states calculated with a constant effective mass, $m_{eff} = m_{red} = 0.92m$ (R_{box} = 28 fm).

	$R_{ljl'j'}^{2_1^+}$						
l_j / $l'_{j'}$	$s_{1/2}$	$p_{1/2}$	$p_{3/2}$	$d_{3/2}$	$d_{5/2}$	$f_{5/2}$	$f_{7/2}$
$s_{1/2}$	-	-	-	-	0.003	-	-
$p_{1/2}$	-	-	0.105	-	-	0.0146	-
$p_{3/2}$	-	0.105	-	0.004	-	-	-
$d_{3/2}$	-	-	0.004	-	-	-	-
$d_{5/2}$	0.003	-	-	-	0.005	-	-
$f_{5/2}$	-	0.0146	-	-	-	-	-
$f_{7/2}$	-	-	-	-	-	-	-

Table 5: Phonon components $R_{ljl'j'}^{2_1^+}$ larger than 0.001, calculated in the wave-function of the ground state of ^{14}C calculated with a constant effective mass, $m_{eff} = m_{red} = 0.92m$ (R_{box} = 28 fm).

Xpp' ; Ypp' and App'2+ amplitudes for 12C + 2n (0+) states: GPV

	$E= 6.87$ $R_{box}=20$ $R^{2_1^+} = 0.623$	$E= 6.91$ $R_{box}=22$ $R^{2_1^+} = 0.729$	$E= 7.14$ $R_{box}=24$ $R^{2_1^+} = 0.728$	$E= 6.96$ $R_{box}=26$ $R^{2_1^+} = 0.613$	$E= 7.11$ $R_{box}=28$ $R^{2_1^+} = 0.785$
l_j	X^2_{lj}	X^2_{lj}	X^2_{lj}	X^2_{lj}	X^2_{lj}
$s_{1/2}$	0.06	0.041	0.03	0.04	0.012
$p_{1/2}$	0.112	0.004	0.001	0.005	0.012
$p_{3/2}$	0.029	0.003	0.056	0.005	0.05
$d_{3/2}$	0.006	0.019	0.007	0.003	0.007
$d_{5/2}$	0.154	0.195	0.179	0.279	0.111
$f_{5/2}$	-	-	-	-	-
$f_{7/2}$	-	-	-	-	-

Table 23: Main 0-phonon components of the wavefunctions of the excited state of ^{14}C carrying the largest S_{dUdr} strength around $E = 7$ MeV for a series of boxes (R_{box} = 20-28 fm).

Note: About 70% on the phononic side!!

$|0^+_n\rangle = \sum_{pp'} (X_{pp'} (n) \,|pp'(0^+)\rangle + Y_{hh'} (n) \,|hh'(0^+)\rangle) +$
$\sum_{pp'\nu} R_{pp'\nu} (n) \,|pp'(2^+)\nu(2^+)\rangle$

Unperturbed

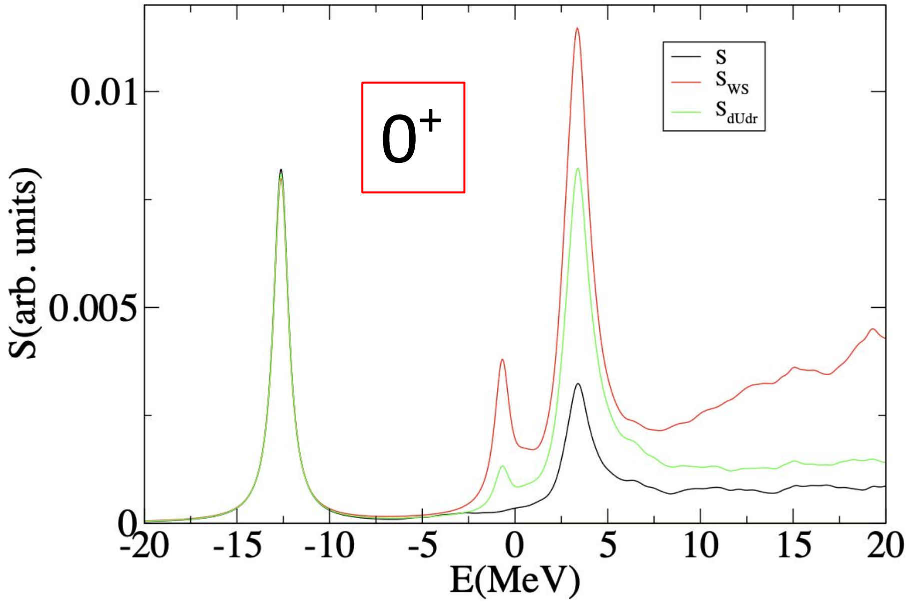

14C

Form factors:

volume

density

surface

Gogny p-p

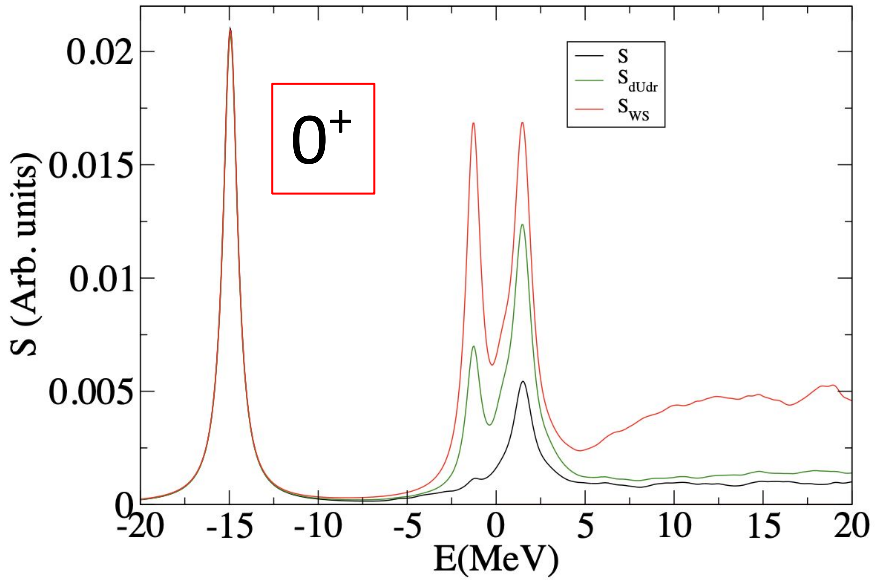

Gogny p-p + phonon coupling

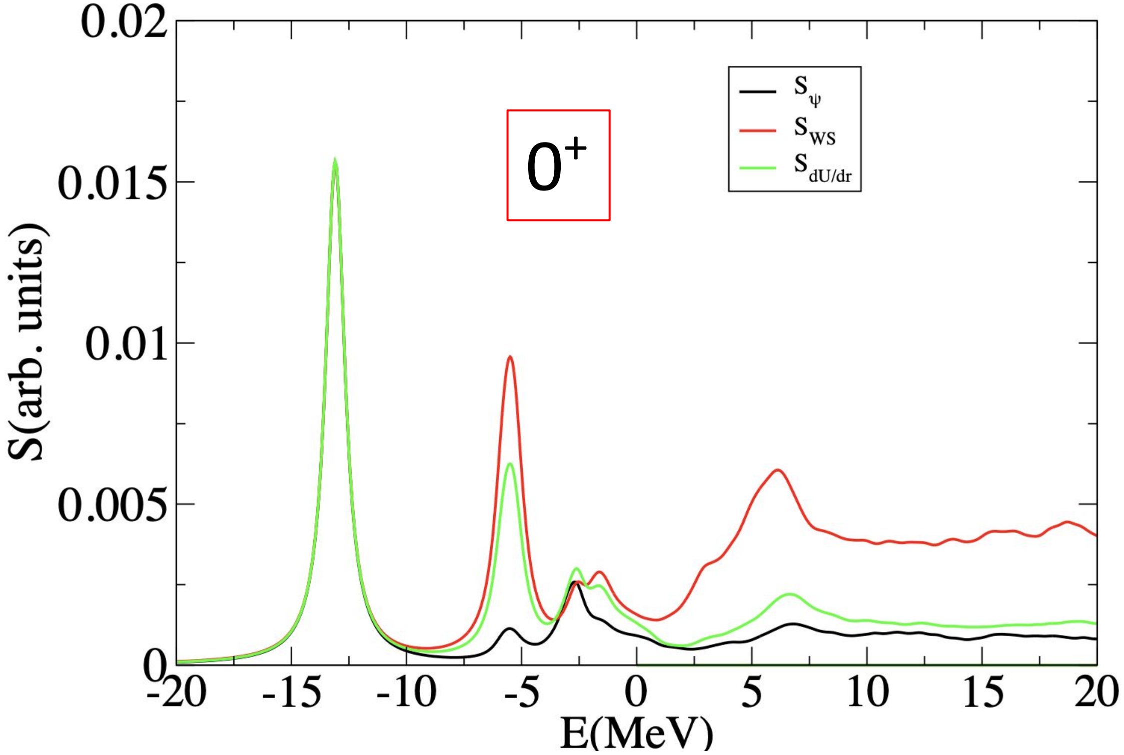

$^{18}O + ^{12}C$ optical potential

S. SZILNER *et al.* PHYSICAL REVIEW C **64** 064614

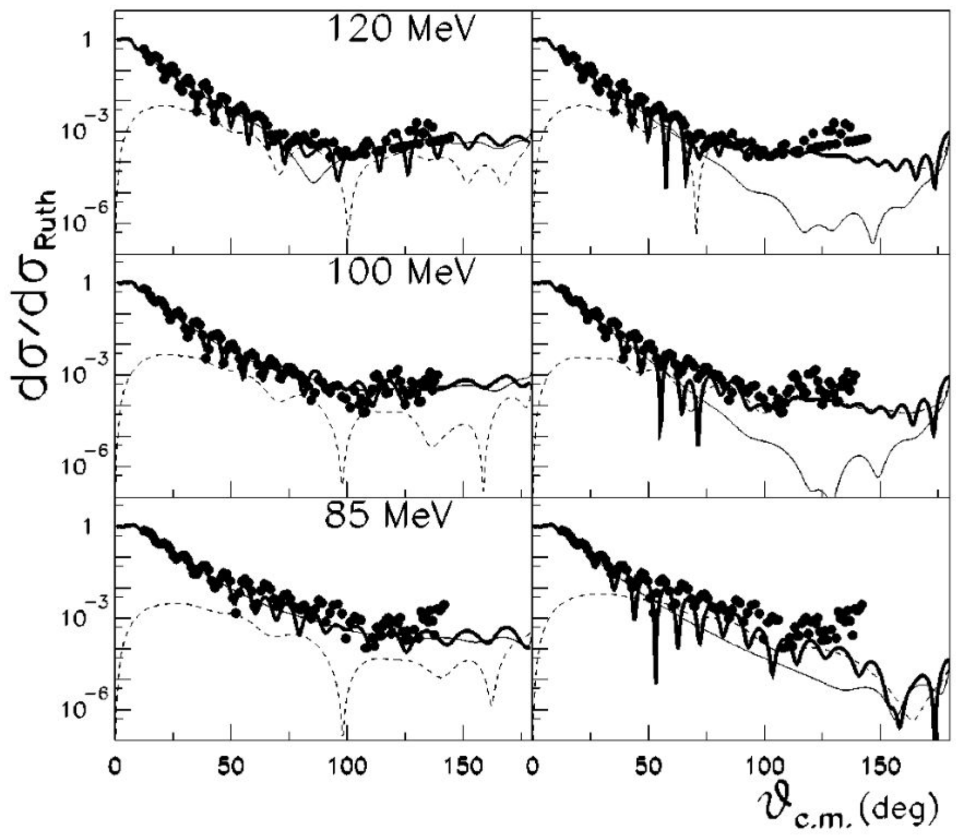

FIG. 2. Same caption as for Fig. 1 but for the $^{18}O + ^{12}C$ elastic scattering at 120, 100, and 85 MeV.

TABLE II. Phenomenological potentials; the real part is a WS2 term and the imaginary part is a WS1 term (pure volume).

E_{lab} (MeV)	$E_{c.m.}$ (MeV)	V (MeV)	W (MeV)	R_W (fm)	a_W (fm)
$^{16}O + ^{12}C$ $R_V = 4$ fm, $a_V = 1.4$ fm					
132	56.6	293	13.4	5.900	0.603
124	53.2	290	14.1	5.712	0.636
115.9	49.7	290	13.0	5.878	0.522
100	42.9	297	10.4	6.079	0.523
94.8	40.6	297	8.8	6.672	0.317
80.0	34.3	297	9.0	6.557	0.322
$^{18}O + ^{12}C$ $R_V = 4.08$ fm, $a_V = 1.38$ fm					
E_{lab} (MeV)	$E_{c.m.}$ (MeV)	V (MeV)	W (MeV)	R_W (fm)	a_W (fm)
120	48	293	13.4	6.443	0.523
100	40	305	13.9	6.270	0.615
85	34	324	18.3	5.930	0.562

$^{12}C(^{18}O,^{16}O)^{14}C(gs)$ at E_{lab} = 84 MeV

2nd order DWBA calculation (G. Potel, Rep. Prog. Phys. 76(2013) 106301)

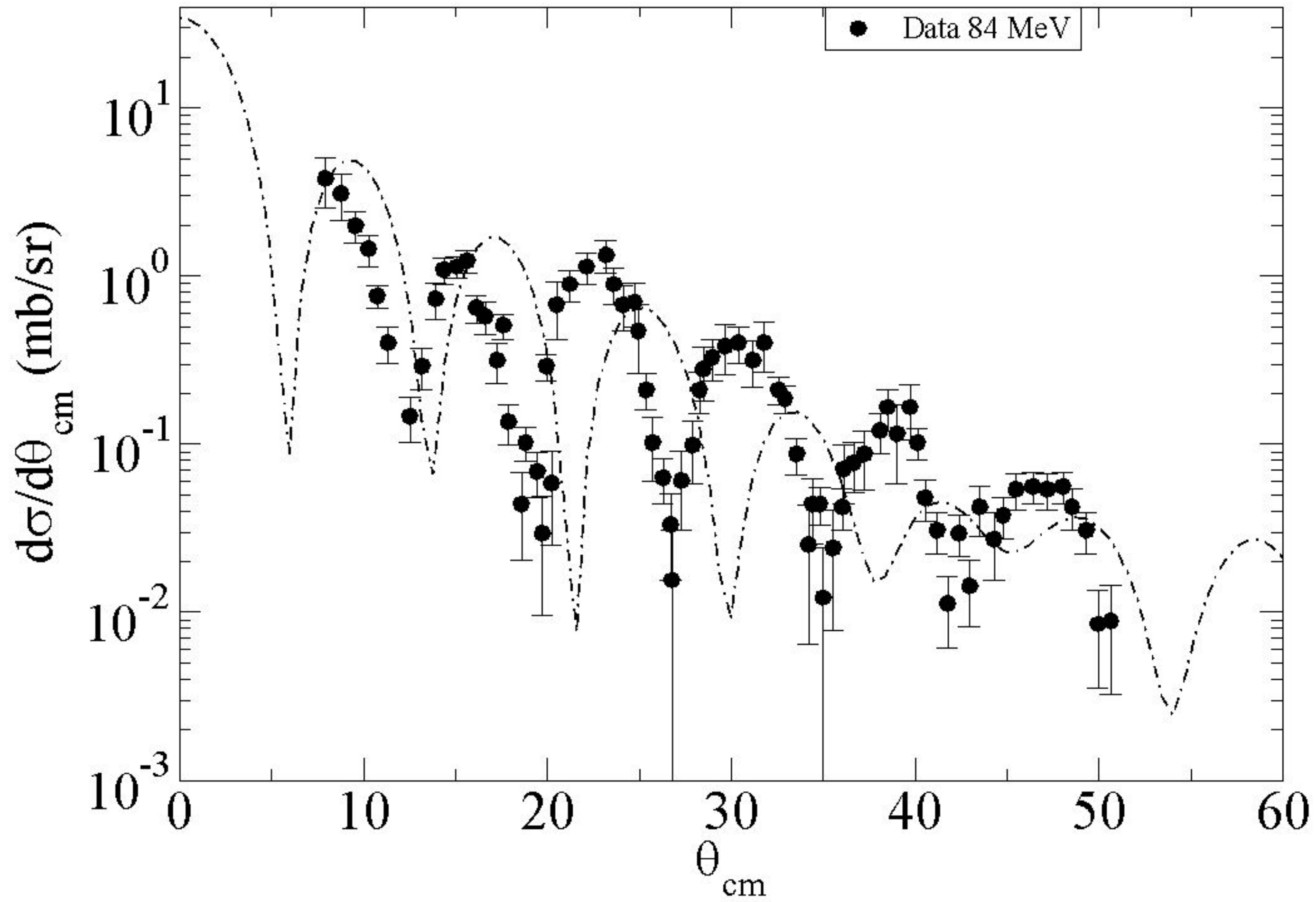

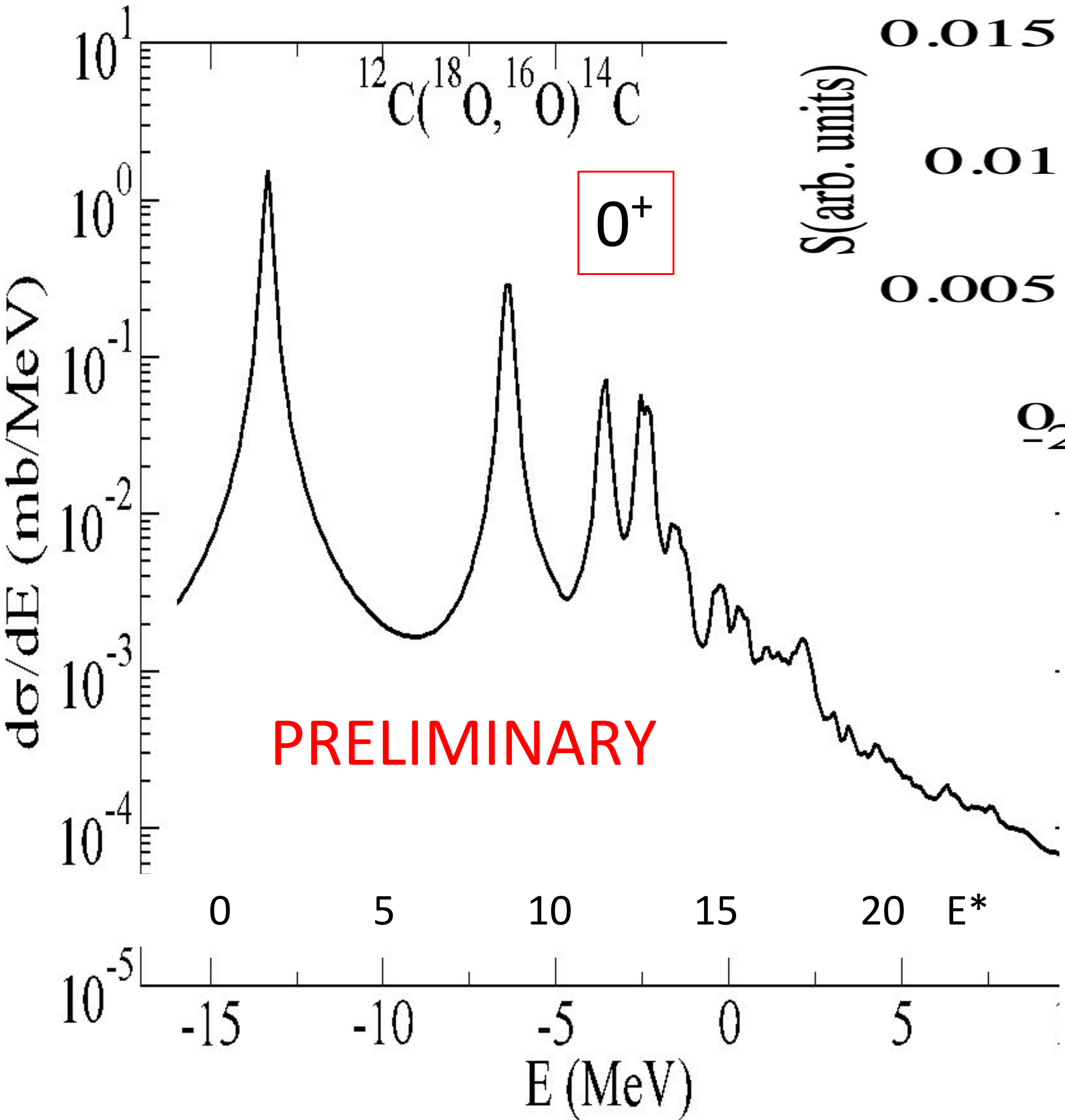

$^{12}C(^{18}O,^{16}O)^{14}C$
0+
PRELIMINARY
dσ/dE (mb/MeV)
E (MeV)
0 5 10 15 20 E*

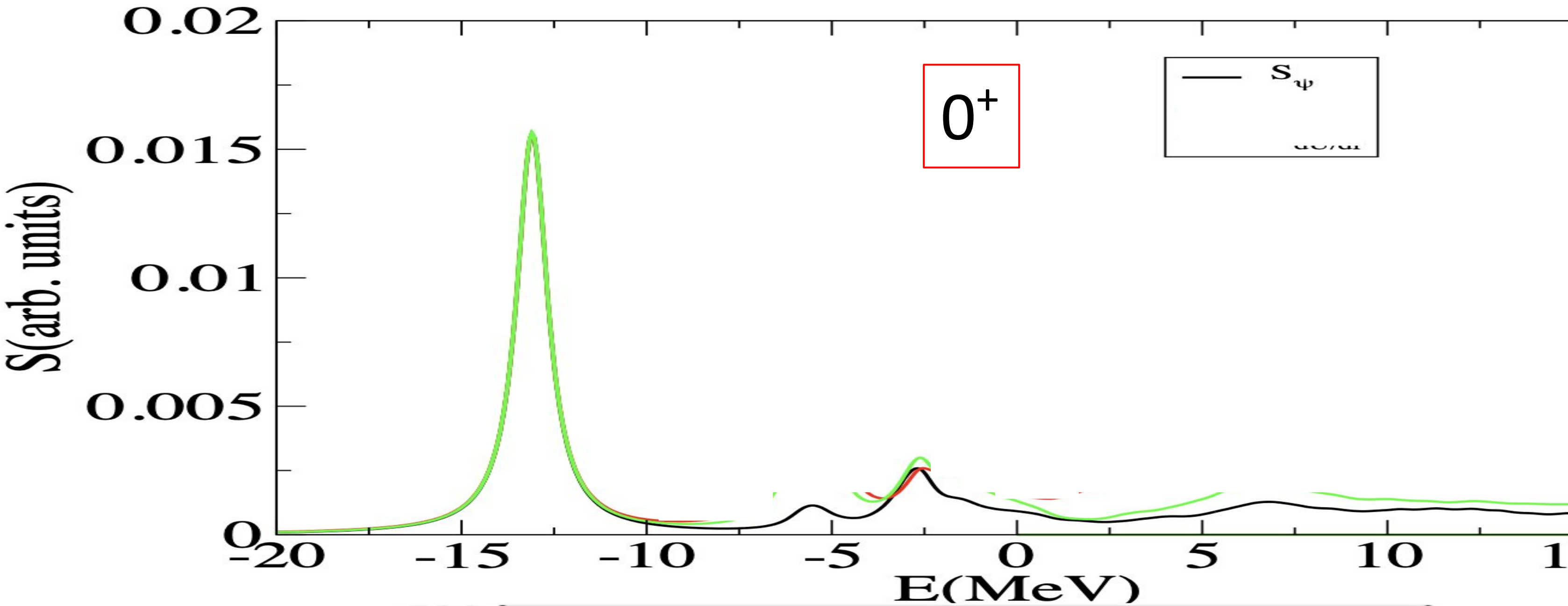

0+
S_ψ
S(arb. units)
E(MeV)

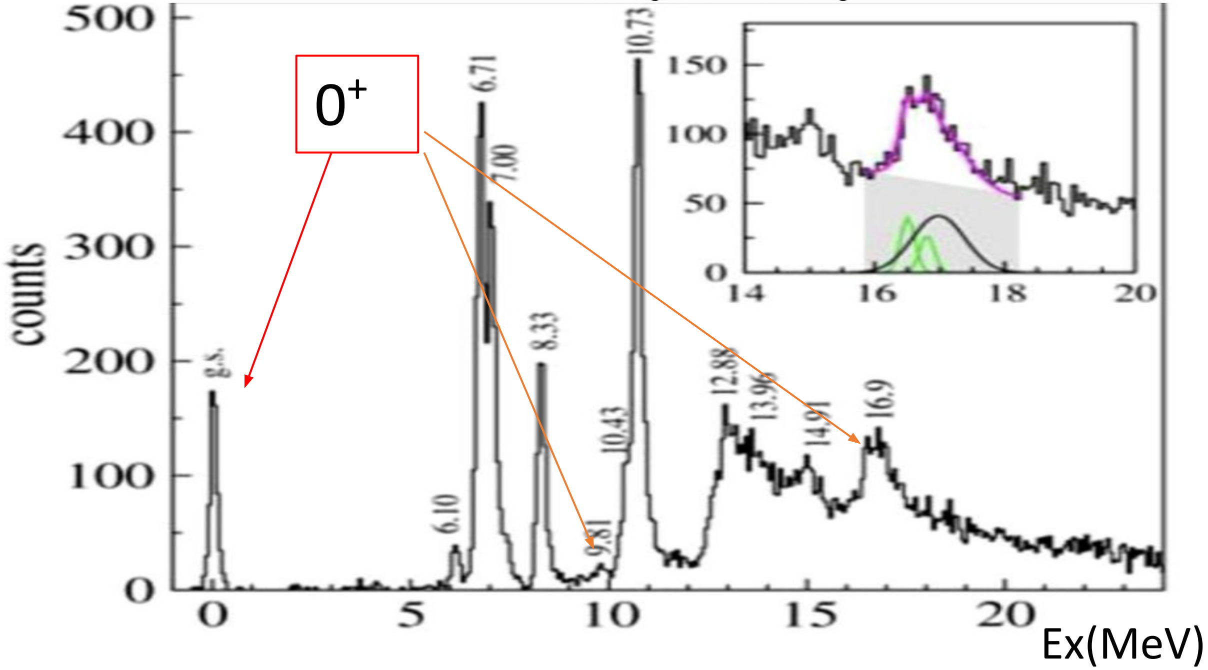

0+
counts
Ex(MeV)
g.s.
6.10
6.71
7.00
8.33
9.81
10.43
10.73
12.88
13.96
14.91
16.9

Comparison with empirical WS(l-dependent)+Gogny

$8 < \theta_{cm} < 35$

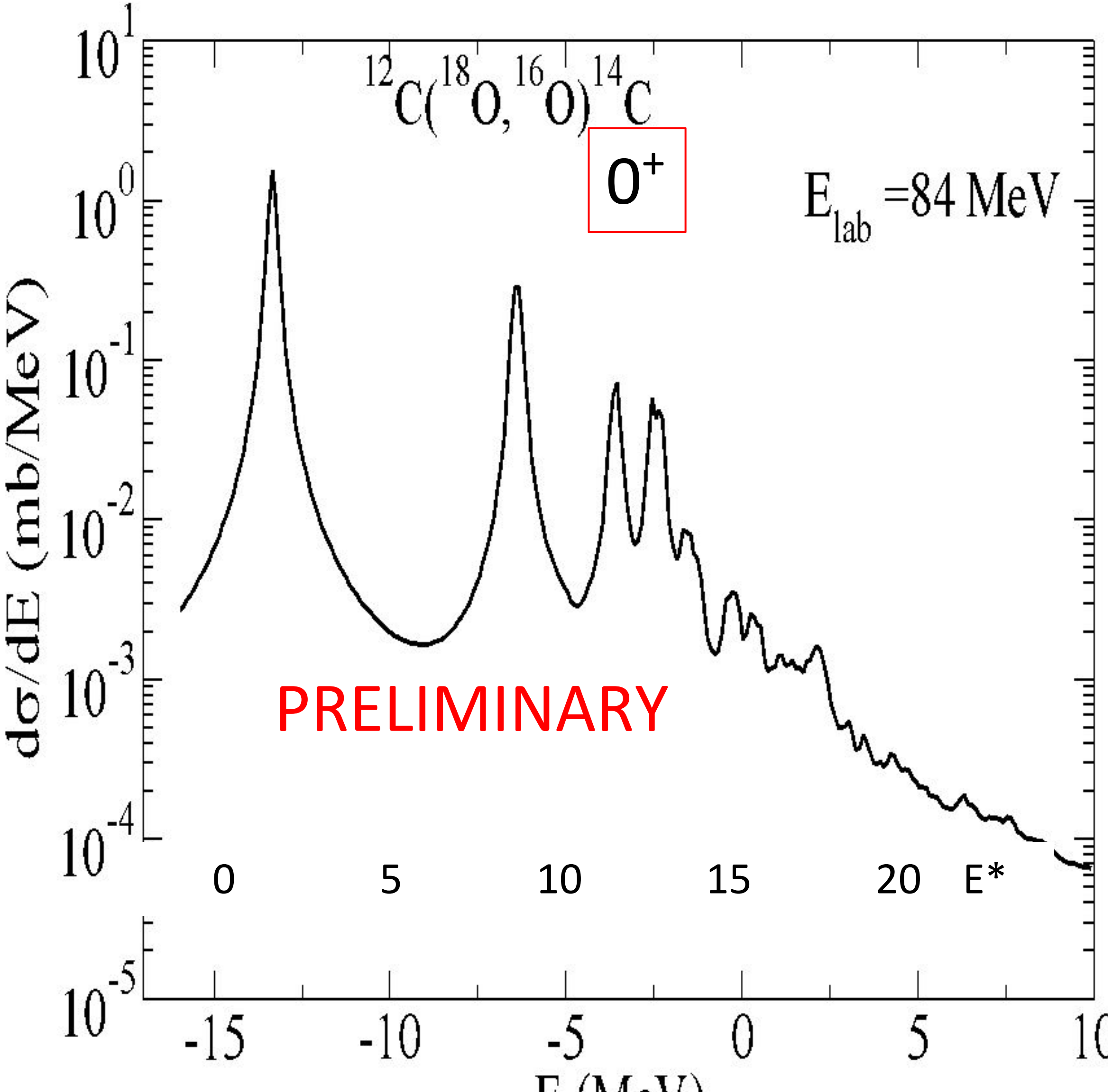

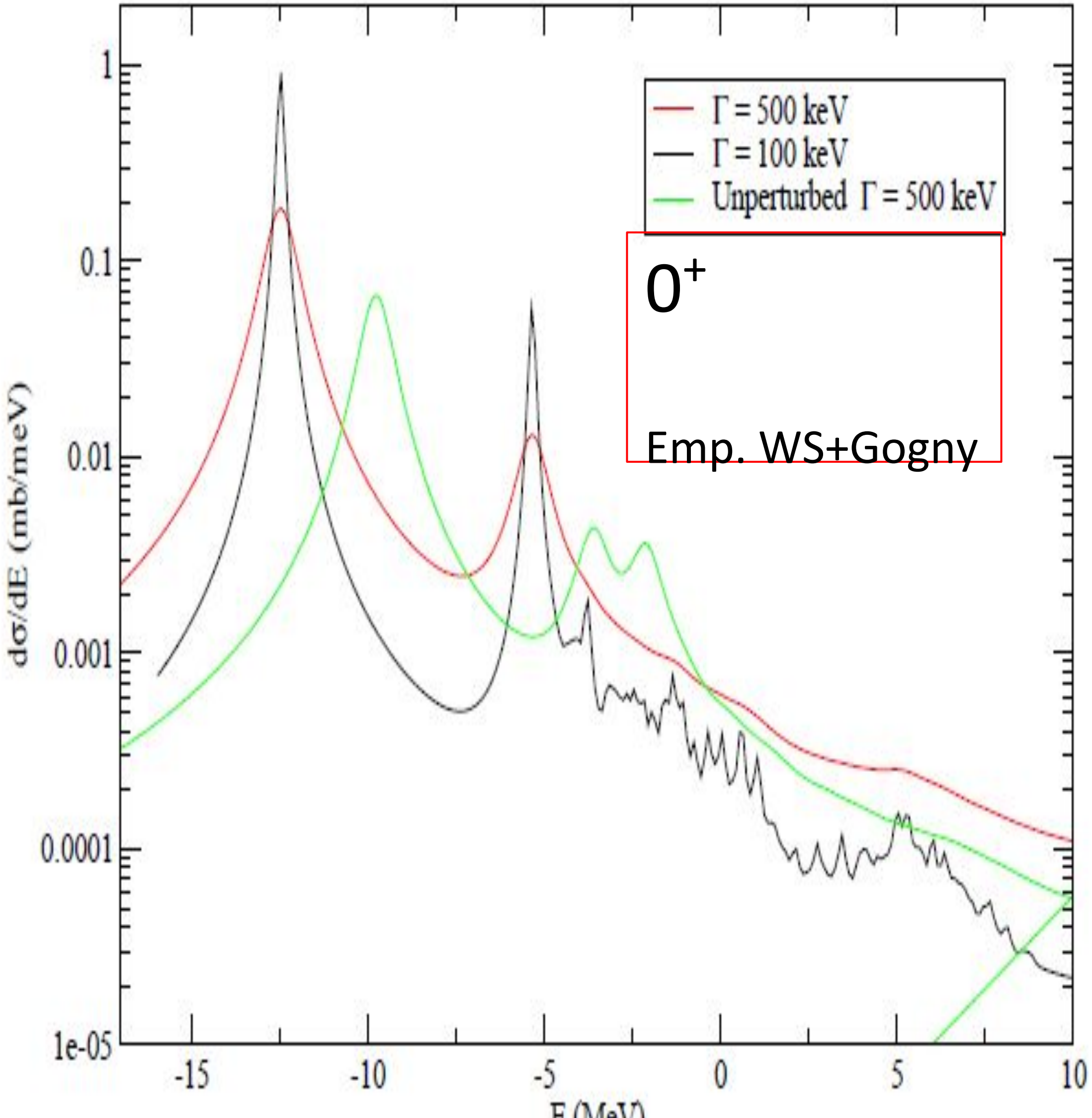

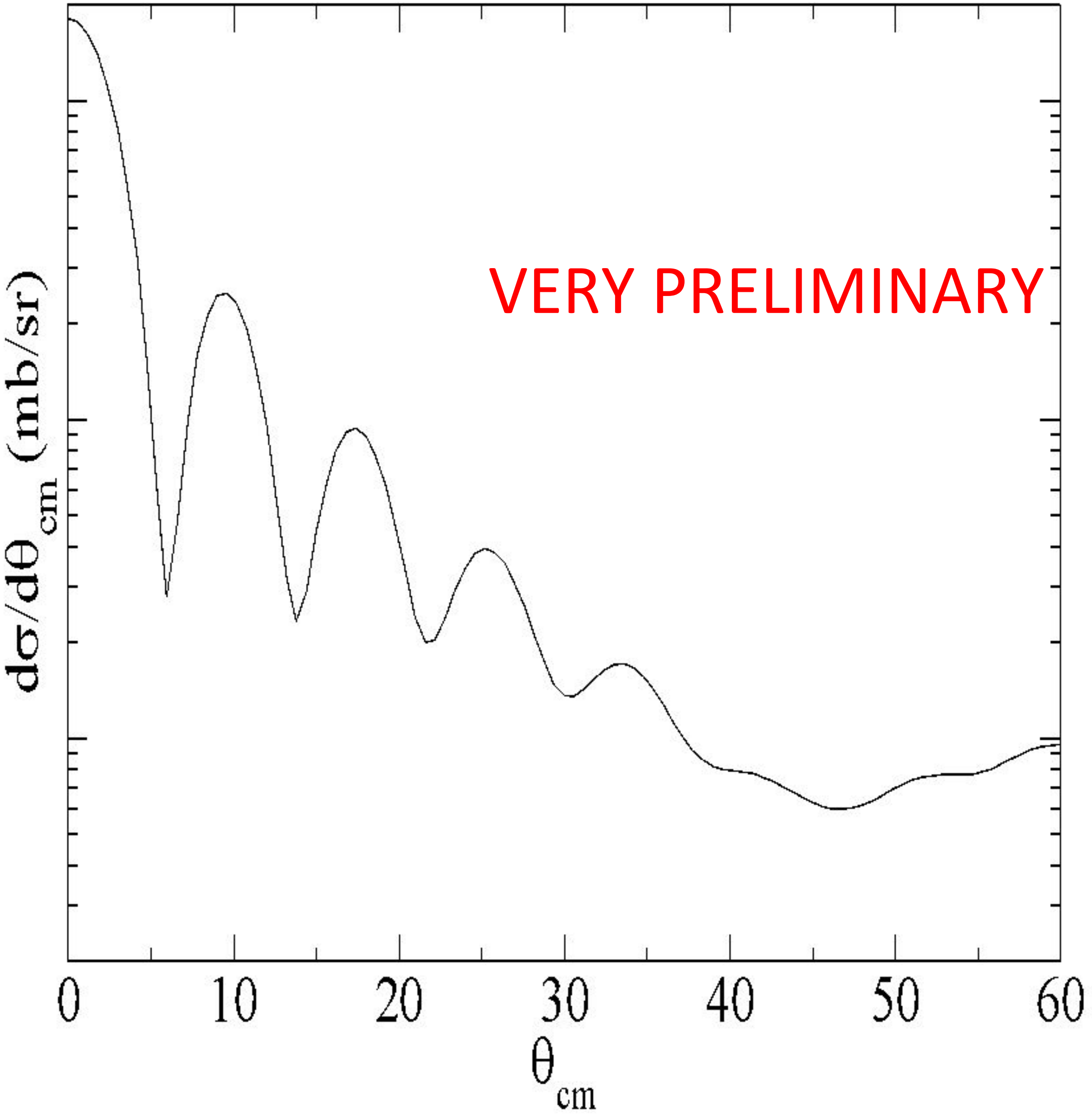
VERY PRELIMINARY
dσ/dθ_cm (mb/sr)
θ_cm
0
10
20
30
40
50
60

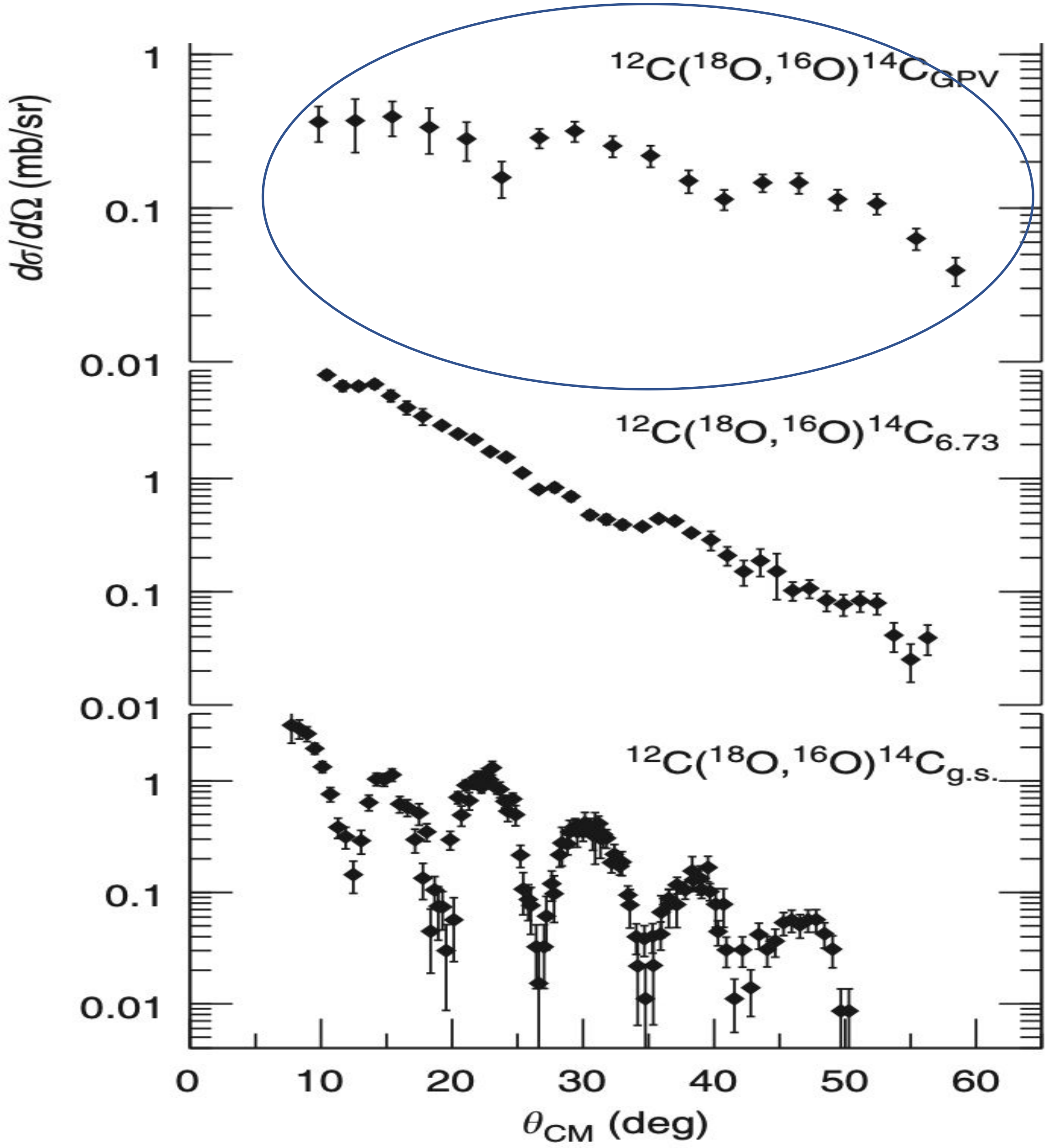
¹²C(¹⁸O,¹⁶O)¹⁴C_GPV
¹²C(¹⁸O,¹⁶O)¹⁴C_6.73
¹²C(¹⁸O,¹⁶O)¹⁴C_g.s.
dσ/dΩ (mb/sr)
1
0.1
0.01
θ_CM (deg)
0
10
20
30
40
50
60

CONCLUSIONS

We have computed the 2n-transfer strength to populate 0+ states in the continuum of 14C
and made the first steps to compute the absolute cross section of the reaction $^{12}C(^{18}O,^{16}O)^{14}C$.
The theoretical model is based on particle-particle RPA extended to include the effects
of coupling to collective quadrupole vibrations, in keeping with previous
calculations of weakly-bound systems.

The aim is to compare our results with the bump and the associated angular distribution
revealed in the excitation spectrum and attributed to the Giant Pairing Vibration.

THANK YOU !!

NFT in two phrases

In the preceding parts of Sec. 6-5, we have considered some of the consequences of the particle-vibration coupling in renormalizing the properties of the elementary modes of excitation and producing interactions between them. The systematic treatment of the particle-vibration coupling amounts to a nuclear field theory, which incorporates in a consistent manner the consequences arising from the fact that the quanta are built out of the same degrees of freedom as are the particle modes of excitation. Thus, the antisymmetry between the particles that are treated explicitly and those that are involved in the collective modes is expressed in terms of

exchange interactions such as that illustrated by Fig. 6-10d (see the comments on p. 428); the inclusion of these exchange interactions at the same time ensures the orthogonality of the states built out of different elementary modes.

NFT basic ingredients

Vertices

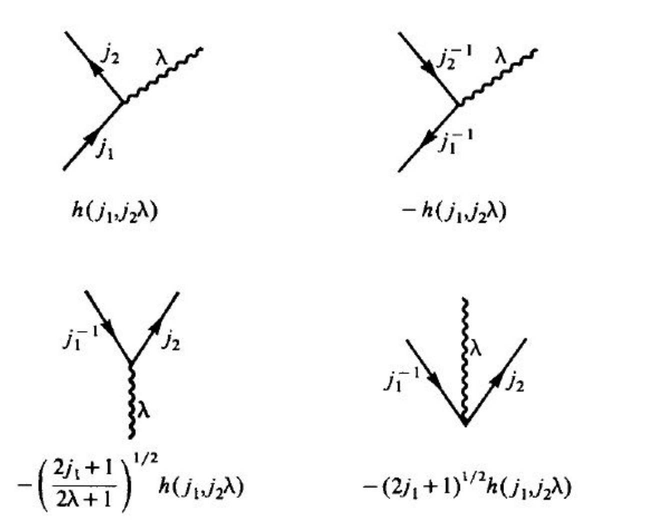

Fermionic lines: HF s-p levels
Phonons (bosons): RPA states

$$h(j_1,j_2\lambda) \equiv \langle j_2, n_\lambda = 1; I = j_1, M = m_1 | H' | j_1 m_1 \rangle$$

$$= (-1)^{j_1+j_2}(2j_1+1)^{-1/2}(2\lambda+1)^{-1/2}\langle j_2 \| k_\lambda Y_\lambda \| j_1\rangle \langle n_\lambda = 1 \| \alpha_\lambda \| n_\lambda = 0\rangle$$

External Operator

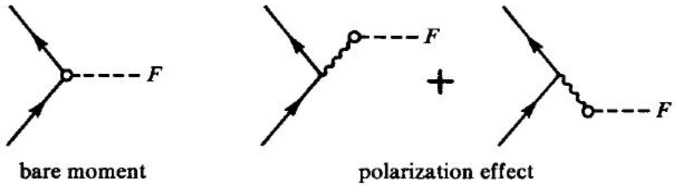

Figure 6-8 Renormalization of single-particle moment resulting from particle-vibration coupling.

NFT rules:

Use Feynman diagrams “alla QED”

BUT

Not those involving fermionic bubbles (overcounting)

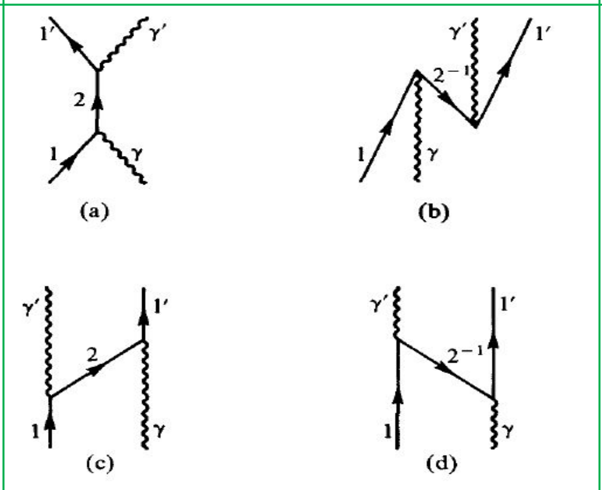

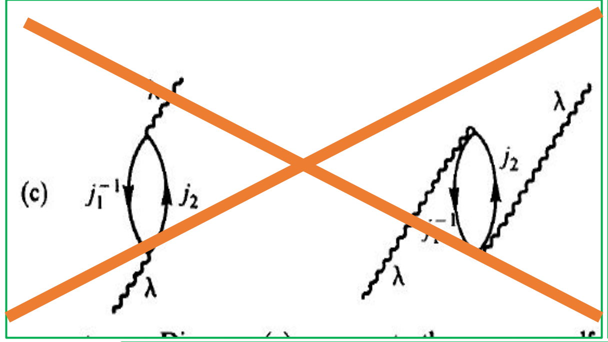

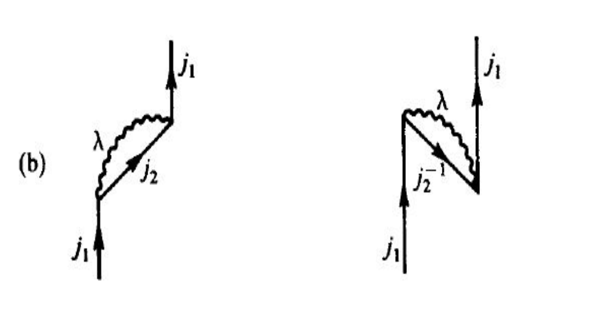

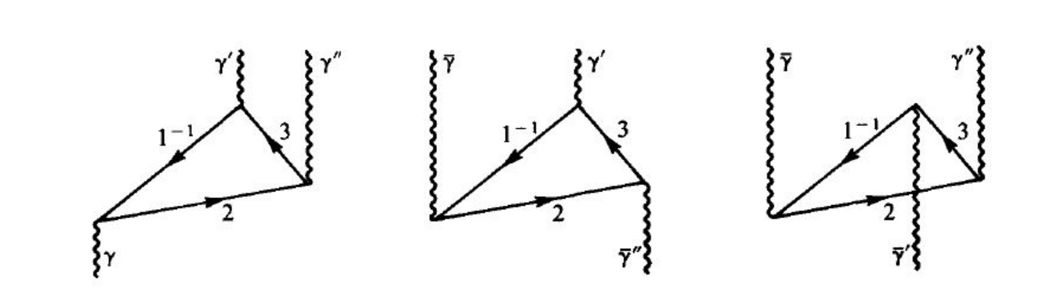

The Phonon Exchange Induced Interaction

6-5f Polarization Contributions to Effective Two-Particle Interactions

In second order, the particle-vibration coupling gives rise to an interaction between two particles, which can be evaluated in a manner similar to

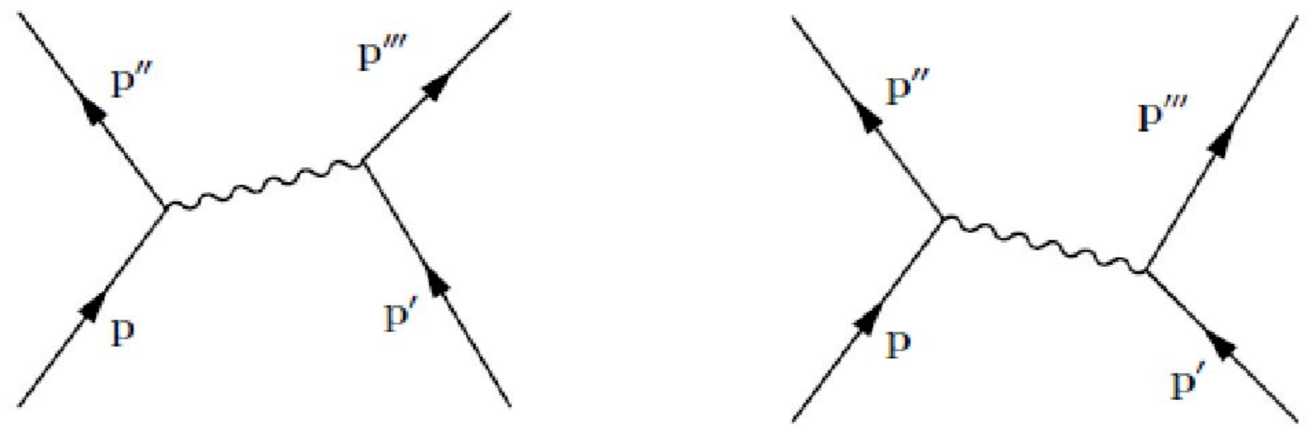

The polarization interaction resulting from the coupling to the low-frequency modes may be considerably larger than the bare force; since the frequencies of these modes may be comparable with the particle frequen-

TDA and Blanchon l-dependent

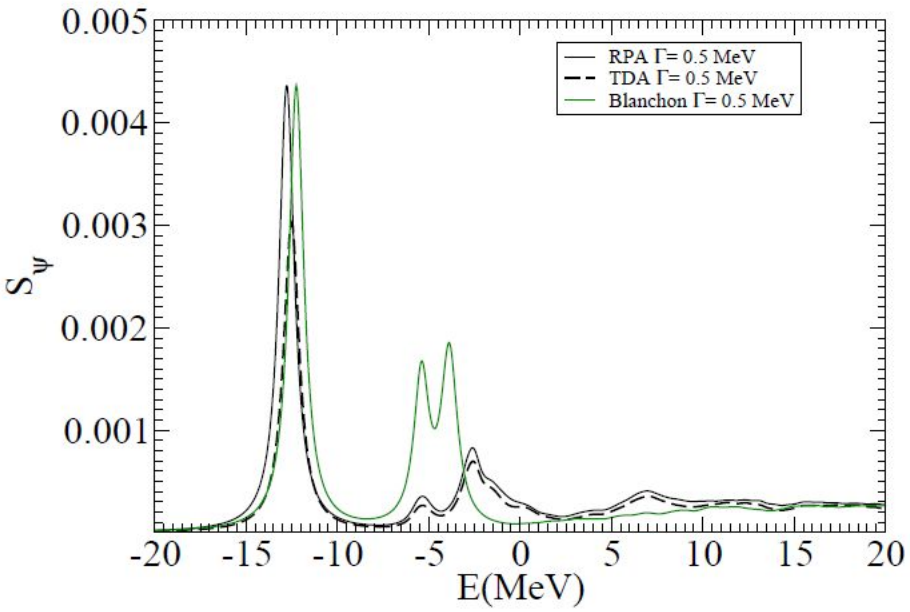

Figure 20: The strength function S_ψ calculated in ^{14}C with the extended pp-RPA equations with the averaging parameter $\Gamma = 0.5$ MeV, already shown in Fig. 19, is compared with the corresponding TDA results. Also shown are the RPA strength functions obtained neglecting the dynamic particle-vibration coupling, and using a $l-$dependent mean field, as discussed in the text. The two RPA strength functions are normalised, so that they coincide for the ground state.

More detail

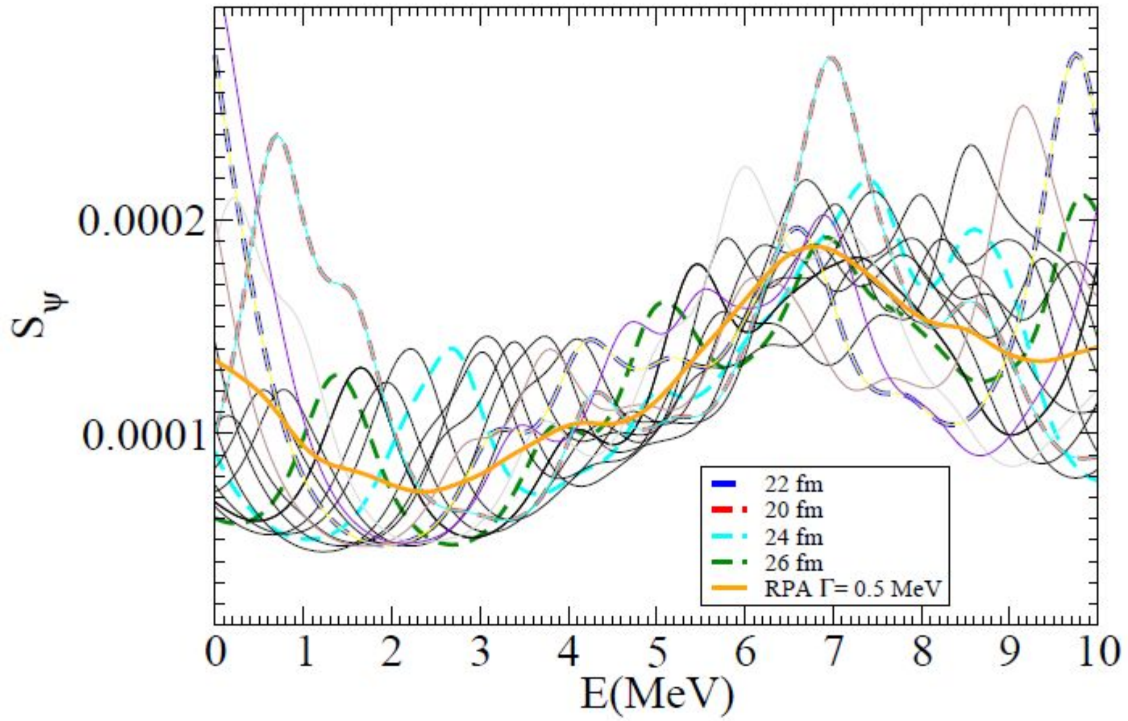

Figure 21: The strength function S_ψ already shown in Fig. 19 is shown by the orange curve in a restricted energy interval. Also shown are the strength functions calculated in the individual boxes, with R_{box} ranging from 20 fm to 28.5 fm with a 0.5 fm step. The boxes corresponding to R_{box} = 20,22,24 and 26 fm are explicitly indicated.

Just Gogny and WS empirical (l-dependent)

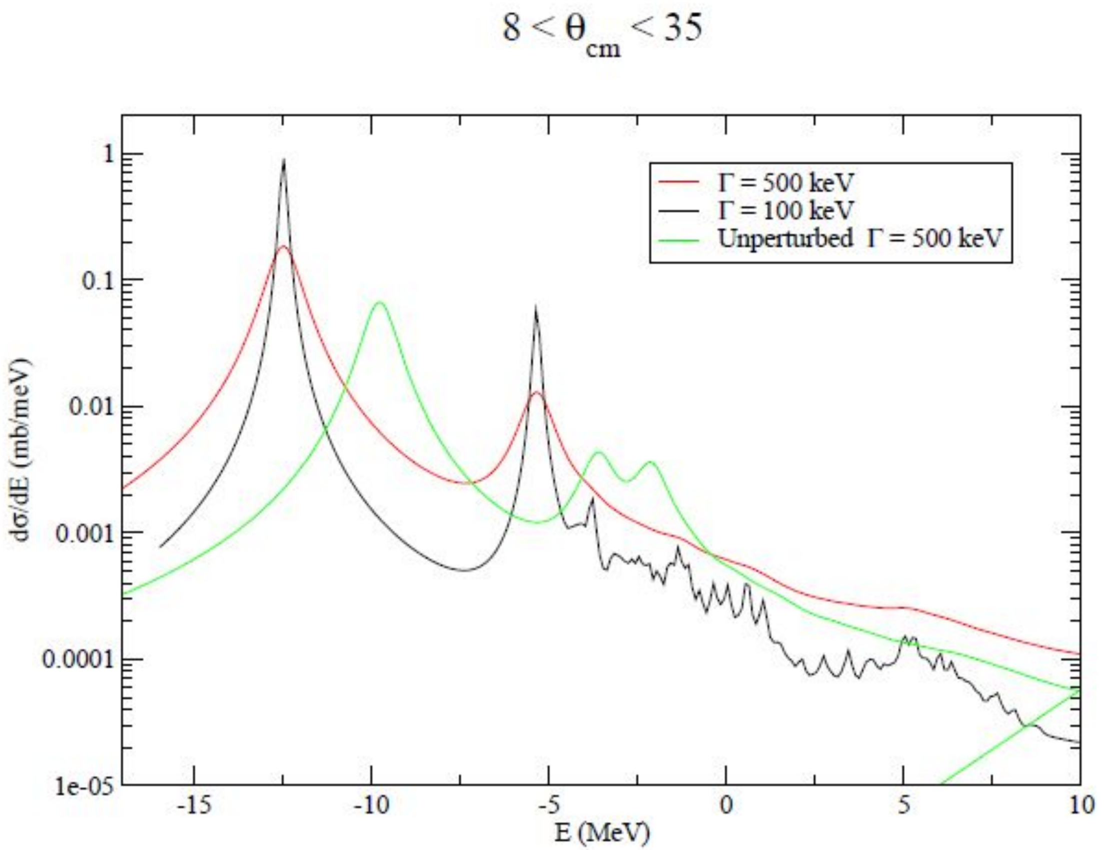

Figure 17: Excitation function obtained taking the average of the excitation functions calculated in different boxes with Γ= 100 keV (shown in Fig. 16) and 500 keV. Also shown is the excitation function obtained from unperturbed states, neglecting the Gogny interaction.

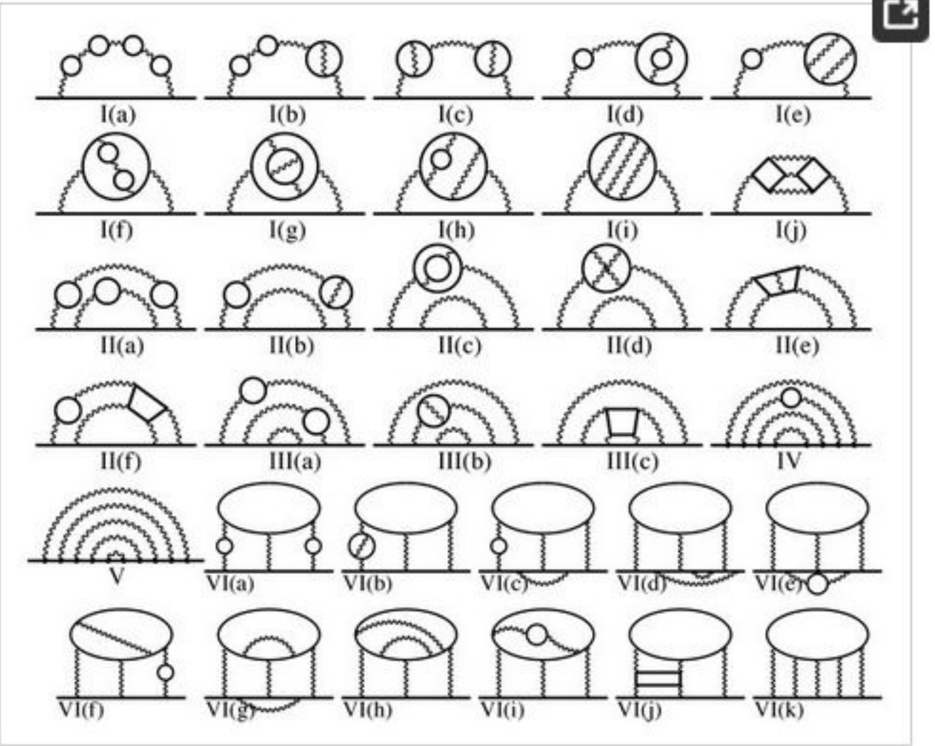

Figure 5. Tenth-order vertex diagrams. There are 12,672 diagrams in total, and they are divided into 32 gauge-invariant subsets over six super sets. Typical diagrams of each subsets are shown as **I**(**a**–**j**), **II**(**a**–**f**), **III**(**a**–**c**), **IV**, **V**, and **VI**(**a**–**k**). There are Set I 208 diagrams (I(a) 1, I(b) 9, I(c) 9, I(d) 6, I(e) 30, I(f) 3, I(g) 9, I(h) 30, I(i) 105, I(j) 6), Set II 600 diagrams (II(a) 24, II(b) 108, II(c) 36, II(d) 180, II(e) 180, II(f) 72), Set III 1140 diagrams (III(a) 300, III(b) 450, III(c) 390), Set IV 2072 diagrams, Set V 6354 diagrams, Set VI 2298 diagrams (VI(a) 36, VI(b) 54, VI(c) 144, VI(d) 492, VI(e) 48, VI(f) 180, VI(g) 480, VI(h) 630, VI(i) 60, VI(j) 54, VI(k) 120). The straight and wavy lines represent electron and photon propagators, respectively. The external photon vertex is omitted for simplicity and can be attached to one of the electron propagators of the bottom straight line in super sets I–V or the large ellipse in super set VI. Reprinted from [12].